**ISTANBUL TECHNICAL UNIVERSITY ★ GRADUATE SCHOOL**

# INVESTIGATION OF THE EFFECT OF DWELL PERIOD IN LOAD CONTROLLED FATIGUE TESTS OF INCONEL 718 SUPERALLOY

**M.Sc. THESIS**

**Numan Berat YONDU**

**Department of Metallurgical and Materials Engineering**

**Materials Engineering Programme**

**FEBRUARY 2022**

**ISTANBUL TECHNICAL UNIVERSITY ★ GRADUATE SCHOOL**

# INVESTIGATION OF THE EFFECT OF DWELL PERIOD IN LOAD CONTROLLED FATIGUE TESTSOFINCONEL 718 SUPERALLOY

**M.Sc. THESIS**

**Numan Berat YONDU**
**(506171422)**

**Department of Metallurgical and Materials Engineering**

**Materials Engineering Programme**

**Thesis Advisor: Prof. Dr. Murat BAYDOĞAN**

**FEBRUARY 2022**

**İSTANBUL TEKNİK ÜNİVERSİTESİ ★LİSANSÜSTÜ EĞİTİM ENSTİTÜSÜ**

# INCONEL 718 SÜPERALAŞIMININ YÜK KONTROLLÜ YORULMA DENEYİNDE BEKLEME SÜRESİNİN ETKİSİNİN İNCELENMESİ

**YÜKSEK LİSANS TEZİ**

**Numan Berat YONDU**
**(506171422)**

**Metalurji ve Malzeme Mühendisliği Anabilim Dalı**

**Malzeme Mühendisliği Programı**

**Tez Danışmanı: Prof. Dr. Murat BAYDOĞAN**

**ŞUBAT 2022**

Numan Berat YONDU, a M.Sc. student of İTU Graduate School student ID 506171422, successfully defended the thesis entitled "INVESTIGATION OF THE EFFECT OF DWELL PERIOD IN LOAD CONTROLLED FATIGUE TESTS OF INCONEL 718 SUPERALLOY" which he prepared after fulfilling the requirements specified in the associated legislations, before the jury whose signatures are below.

| | | |
|---|---|---|
| **Thesis Advisor :** | **Prof. Dr. Murat BAYDOĞAN**<br>Istanbul Technical University | ..... |
| **Jury Members :** | **Prof.Dr. Hüseyin ÇİMENOĞLU**<br>Istanbul Technical University | ..... |
| | **Assoc.Prof. Sebahattin KIRTAY**<br>Istanbul University Cerrahpaşa | ..... |

**Date of Submission : 13 January 2022**
**Date of Defense : 03 February 2022**

***To my family and Turkish enlightenment***

## FOREWORD

I would like to thank Prof. Dr. Murat BAYDOĞAN for his guidance, encouragement and valuable suggestions to complete the study of this thesis.

I would also like to thank Cengiz KOCALAR, Ramazan ALTAŞ, Ethem ŞENOL, İlker ADALI, Zeliha İdil KARA, Göktuğ KARA, Ali Fırat DİNLER, Umutcan ERTÜRK, Furkan ÖZKAYA, Gözde Ergün AĞDACI, Rabia GÜNAY and Hasan Fehmi ÇAPIN for their practical support and helping me through my studies at TUSAS ENGINE INDUSTRIES.

Finally, I would like to thank my family for their endless support and patience during my thesis work.

January 2022

Numan Berat YONDU
(Metallurgical and Materials Engineer)

**TABLE OF CONTENTS**

**Page**

**ABBREVIATIONS**

**$\bar{y}$** **:** Average of observed life

**A** **:** Load/Stress A ratio

**AMS** **:** Aerospace Material Specifications

**ASTM** **:** American Society for Testing and Materials

**BCT** **:** Body Centered Tetragonal

**Dc** **:** Critical Value of calculated Durbin Watson Calculation

**DE** **:** Dynamic Enbrittlement

**Di** **:** Durbin Watson Calculation

**FCC** **:** Face Centered Cubic

**HCF** **:** High Cycle Fatigue

**HT** **:** High Temperature

**IHPTE** **:** Integrated High Performance Turbine Engine Technology

**ISO** **:** International Organization Of Standardization

**Ka** **:** Surface Condition Factor

**ka-kb-kc-kd-ke-kf :** Endurance limit modification factors indicating different working conditions

**LCF** **:** Low Cycle Fatigue

**M3B2** **:** Tetragonal lattice forming with Borides

**MMPDS** **:** Metallic Materials Properties Development and Standardization

**NADCAP** **:** National Aerospace and Defense Contractors Accreditation Program

**NCR** **:** Normalized Cycle Ratio

**No** **:** Observed Life

**Np** **:** Predicted Life

**PWR** **:** Plastic Work Capacity

**R** **:** Load/Stress ratio

**$R^2$** **:** Coefficient of determination

**RSME** **:** Root mean square error for entire sample

**RT** **:** Room Temperature

**S'e** **:** Test Specimen Endurance limit

**Sa** **:** Stress Amplitude

**SAGBO** **:** Stress Accelarated Grain Boundary Oxidation

**SC** **:** Single Cristal

**SD** **:** Standard Deviation

**Se** **:** Endurance Stress

**SEM** **:** Scanning Electron Microscopy

**Sm** **:** Mean Stress

**Smax** **:** Maximum Stress

**Smin** **:** Minimum Stress

**SR** **:** Standardised Residual

**Sr** **:** Stress/Strain Range

**SSR** **:** Summation of Squared Residuals

**Sut** **:** Ultimate Tensile Stress

**Ti** **:** Studendized t distribution

**USAF** **:** United States Air Force

**USN** **:** United States Navy

**Yi** **:** Observed Result

## LIST OF TABLES

**Page**

**LIST OF FIGURES**

**Page**

## INVESTIGATION OF THE EFFECT OF DWELL PERIOD IN LOAD CONTROLLED FATIGUE TESTS OF INCONEL 718 SUPERALLOY


### SUMMARY

The use of nickel alloys has become widespread in many industries during this last century, nickel with its alloys providing relatively better mechanical properties than conventional ferrous alloys for various industrial applications. Especially with its decent high-temperature oxidation and mechanical resistance makes this alloy the material of choice for engine applications. An example of a mostly used alloy in turbine engine hot sections is Inconel 718 is a niobium-modified and nickel-based superalloy that will be examined in this work.

Inconel 718 superalloy is a face-centered cubic latticed nickel-chromium alloy that can relatively retain its good mechanical strength up to 649°C. These superior mechanical properties are provided with γ″-Ni3Nb precipitate phases present in the structure of the alloy, above mentioned 649°C temperature level secondary δ phase formation causes rapid strength loss of the material.

In industrial applications materials are exposed to various hazardous factors and these can be exemplified as; temperature, residual stresses, corrosion, etc. Depending on the application type these hazardous factors generate different types of deformations can be summed as; creep, fatigue, overload failure, etc. Unlike commonly known deformation types, the exampled engine application of this alloy includes different factors.

In this study, the mechanical property of Inconel 718 is examined in terms of fatigue behavior. The main concern of this work is to determine the material's fatigue properties under pure bending and different conditions. Test conditions will include room temperature, 450°C, and dwell times to simulate material's real usage in the engine application. Additional to fatigue testing hardness measurements and nanoindentation testing were performed at ambient temperature. Fractographic and microstructural examinations of the tested specimens are performed with an optical microscope and SEM (scanning electron microscope) to understand the material's reaction for different deformation factors. To understand the material's mechanical behavior first room temperature and high-temperature load controlled fatigue tests without dwell application have been performed. Parameters are selected to examine mainly the dwell effect on the material by maximizing the dwell cycle.

It is observed that Inconel718 alloy’s dwell sensitivity is depending on temperature and applied stress, change in mechanical properties is also observed with hardness testing. Fractographic examinations have shown that different features become visible under different test conditions. In this work in addition to mechanical testing statistical analysis is also studied for observed data sets.

# INCONEL 718 SÜPERALAŞIMININ YÜK KONTROLLÜ YORULMA DENEYİNDE BEKLEME SÜRESİNİN ETKİSİNİN İNCELENMESİ

## ÖZET


Geçtiğimiz yüzyıl boyunca Nikel alaşımlarının farklı endüstrilerde kullanımı giderek artış göstermiştir. Nikel alaşımları ile birlikte geleneksel demir bazlı alaşımlara görece daha iyi mekanik özellik gösterdiği bu nedenle de birçok farklı endüstride kullanımı yaygınlaşmıştır.

Özellikle Nikel alaşımlarının yüksek sıcaklık oksidasyon ve mekanik direnci bu malzemeyi motor uygulamalarında tercih edilmesine sebep olmuştur. Türbinli motorların yüksek sıcaklıklı bölgelerinde yaygın olarak kullanılan Nb/Cr katkılı nikel süper alaşımı olan Inconel718 örnektir. Bu çalışmada bu malzemenin mekanik davranışları üzerinde durulmuştur.

Inconel718 süperalaşımı yüzey merkezli kafes yapısına sahip olup Nikel Krom Nb bazlı süper alaşımıdır, bu alaşım 649°C derecelere kadar iyi mekanik özelliklerini koruması ile tercih edilen malzeme olmuştur. Bu yüksek mukavemet özellikleri yapısında bulunan $\gamma''$-$Ni_3Nb$ çökeltiler ile sağlanır. Belirtilen sıcaklık değeri 649°C derece ikincil $\delta$ fazlarının oluşmasını bu da bu sıcaklıktan sonra ani mukavemet düşüşlerinin gözlemlenmesine sebep olur.

Endüstriyel uygulamalarda malzemeler ömürleri üzerinde tehlikeli olabilecek çeşitli koşullara marus kalırlar örnek olarak; yüksek sıcaklıklar, kalıntı gerinimler, korozyon vb. Uygulamaya bağlı olarakta bu tehlikeli koşullar farklı tiplerde hasarlara yol açarlar bunlar; sürünme, yorulma, aşırı yüklenme ani kırılması vb olarak örneklendirilebilir. Bunlardan farklı olarak da motor uygulamalarında kullanılan bu alaşım bu örneklendirilen koşullarından daha farklı tesirler altında da çalışırlar.

Bu çalışmada Inconel718'in mekanik özellikleri yorulma davranışı merkezli olacak şekilde incelenmiştir. Bu çalışmanın ana unsuru malzemenin eğme baskın olacak şekilde yorulma davranışı üzerine durulmuştur, bu duruma ilaveten farklı parametrelerde dahil edilmiştir. Test koşulları oda sıcaklığı, 450°C derece atmosfer koşullarının yanı sıra bekleme periyodlarının çevrimsel yüklemeli teste dahil edilmesi ile malzemenin motor koşullarına daha yakın olarak simüle edilmesi için planlanmıştır.

Yorulma testlerinin yanında sertlik ölçümleri, nano indentasyon testleri gerçekleştirilmiştir. Fraktorafik ve mikroyapısal incelemelerde optik mikroskop ve SEM (taramalı elektron mikroskobu) kullanılmıştır. Bu incelemelerle malzemenin farklı koşullar altında nasıl tepki gösterdiğini anlamak için yoğun olarak çalışılmıştır.

Testlerde malzemenin standard koşulda mekanik özelliklerini anlamak için öncelikli olarak oda sıcaklığı yük kontrollü yorulma testleri gerçekleştirilmiştir. Buna mukabil yüksek sıcaklık testleri ve bu testlere bekleme periyotları ve bekleme süreleri yüksek streslerde harcanaca sürelerin etkisini en yüksek seviyeye çıkaracak şekilde planlanmıştır.

En yüksek yüklerde uygulanan bekleme süreleri malzemenin havacılık motorlarında etkisi altında kaldıkları seyir yüklerini simüle etmek bu seyir yüklemelerinin yanı sıra motor başlatma ve durdurma çevrimlerini ele almak için malzemede çevrimsel ve statik yüklemeleri aynı anda yapılarak sağlanmıştır. Bu bekleme sürelerinde normal şartlarda statik yüklemelerde görülen sürünme, oksidasyon, statik toparlanma, tekrar kristalleşme mekanizmalarını tespit edebilmesi için nano indentasyon, sertlik testleri ve mikro yapı çalışmaları hasara uğrayan her numune için uygulanmıştır.

Test uygulamarına ek olarak literatür karşılaştırmaları bu çalışma kapsamında önemli yer almaktadır. Bu literatür araştırmalarında yorulma çevrimlerinin kesintiye uğratılmasıyla başlayan dinamik test içinde statik yüklemelere önem verilmesi son yüzyılda mühendislik uygulamarının ve özellikle motor teknolojilerinin gelişmesi ile son yüzyılda ayrıntılı olarak çalışılmıştır. Bu çalışmalar dinamik yüklemelerin kesintiye uğratılması ile başlayıp günümüzde de eksenel yüklemeler altında çatlak ilerleme testleri ile halen devam edilmektedir.

Eksenel yorulma ve yorulma çatlak ilerleme testleri malzemenin dinamik davranışlarını anlamada yaygın ve etkili olarak kullanılan test yükleme yöntemidir. Dinamik eğme testleri de havacılık motorlarında kullanılan hareketli ve titreşime maruz kalan parçaları simüle etmek için çalışma koşuluna da bağlı olarak eksenel testlere denk ve daha mühim özellikleri tanımlar. Akademik çalışmalardan farklı olarak bu çalışmada bekleme süreleri eksenel yüklemelerden ziyade eğme yüklemeleri özelinde çalışılmıştır.

Yapılan akademik çalışmalarda özellikle bazı malzemelerin test sıcaklıklarına da bağlı olarak ömür değerlerinin önemli derecelerde etkilendiği gözlemlenmiştir. Eksenel yükleme altında yapılan çatlak ilerleme testlerinde de Nikel alaşımlarında da çatlak ilerleme hızlarının arttığı bununda ömür değerlerini yine düşürücü etkilediği gözlemlenmiştir.

Bu çalışmalarda oksijen difüsitesine bağlı olarak çatlak ilerlemelerinde oksidasyona bağlı mekanizmalar gözlemlenmiştir. Bunlar dinamik gevrekleşme ve gerilme tesirli tane sınırı okidasyonları olarak tanımlanmıştır. Çalışmalarda anlaşılan test sıcaklıkları yüksedikçe bekleme süreleri ile de birlikte malzemede belirtilen oksdasyona bağlı mekanizmalara ilaveten sürünme fenomeninde görülen boşluk oluşumu ve yüzey için çatlak başlangıçları bu test koşullarında beklenen bir durumdur.

Çalışmamızda seçilen test sıcaklığı Inconel718'in en yüksek çalışma sıcaklığından uzak ancak motor koşullarında maruz kaldığı bir sıcaklık seçildiği için sürünme mekanizmaları öncelikli olarak beklenmemiştir.

Yükleme koşulunun değişmesi ile bekleme sürelerinde gözlemlenecek metalurjik olguların nasıl etkileneceği sorusunun akademik çalışmalarda yeteri ile çalışılmamış olması bu çalışmanın motivasyonu olmuştur.

Yapılan çalışmanın sonunda Inconel718 malzemesinin yüksek çevrimli yorulma koşullarında sıcaklığa bağlı yumuşama gösterdiği gözlemlenmiştir. Bekletme sürelerinin malzemenin yorulma davranışına etkisinin uygulanan gerilmeye bağlı olduğu düşük gerilmelerde Inconel718 malzemesinin bekletme sürelerine hassas olduğu görülmüştür. Çalışmada eğme koşulunda bekleme süresinin sıcaklığa bağlı olarak hem ömrü arttıran hem de azaltan sonuç verdiği görülmüştür.

Bekleme süresi uygulanan test numunelerinde kırılma yüzeyindeki topografik değişik malzemelerin kırılma mekaniklerinde değişim gerçekleştiği sonucuna varmamızı sağlamıştır.

Yorulma testlerine ek olarak yapılan nano indentasyon testlerinde malzemedeki ömür değişimine rağmen bekleme süresi etkisi ile malzemenin plastik kabiliyetinde bir değişim olmadığı gözlemlenmiştir. Sonuç olarak bekleme sürelerinin tesiri ile 450°C'de yorulma ömründe artış oda sıcaklığında da ömür düşüş görülmüştür.

# 1. INTRODUCTION

Scientific developments in various industries also improve the engineering requirements of its applications. For example advancements in engine technologies also encouraged advances in material technologies to meet engine application's needs. Advances in aviation and internal combustion engine technologies in the past 20th century have also been encouraged to produce new types of alloys rather than ferrous for specific needs. Nickel and Cobalt-based alloys have been started to be used more often for relatively more challenging conditions. Nickel-based alloys with their relatively superior high-temperature mechanical and oxidation resistance made it especially preferred in turbine parts in gas turbine engines. In most cases, despite its good high-temperature mechanical properties Nickel alloys tends to deform under harsh conditions, to delay the inevitable deformation certain protective applications like ceramic coating or cooling systems can be applied [1].

Different protective applications can be applied to prevent system failure, however preventative solutions can be determined in the design step of the part material. Understanding the behaviors of the material under expected conditions is crucial for material design. In gas turbine engines, materials are exposed to many different deformation factors. These can be vary depending on materials service conditions, for Nickel-based turbine parts, mostly moving parts can be exposed to creep, fatigue, corrosion deformation modes. For understanding material behavior various procedures can be applied in terms of mechanical properties tensile tests, creep tests and constant amplitude fatigue tests are applicable. These types of tests examine deformations factors on their own, the test results of these tests can be helpful however to simulate near service conditions on the material, additional parameters can be added to these standard test methods [1].

Fatigue behaviors of rotating parts of the turbine engines are the main concern in designing. There are different methods to determine the materials fatigue behavior such as load-controlled axial fatigue test, strain-controlled fatigue test, rotating bending fatigue test, ultra-high cycle ultrasonic fatigue test, and so on. These different

test methods can result differently from each other because of the nature of these tests, Rotating bending fatigue test is still a relatively promising test method with its easy application for rotating materials. To understand the Nickel-based alloy

behavior in simulated conditions additional parameters like dwell time and dwell frequency were added to standard rotating bending fatigue test under different temperatures [1].

In this study, nickel-based superalloy Inconel718 is tested under a load-controlled rotating bending test to understand materials fatigue behavior. Different temperatures and additional parameters were applied to the test to simulate the service conditions.

## 2. SUPERALLOYS

With the increasing demands for the performance and efficiency of the jet engines, increasing the engine operating temperature became inevitable.

However, in terms of increasing temperatures, there is only one limiting factor and that is the heat resistance of the engine material. To meet that requirement the term Superalloy comes to us. This widely used term is to define a group of metallic alloys which are based on nickel, cobalt, iron with a greater amount of alloying elements than commercially produced traditional engineering alloys.

Traditional engineering alloys focuses on one main alloying element and aims to improve the mechanical and chemical properties of that main element, superalloys on the other hand not only show the main element properties but also aim to show other alloying elements mechanical or/and chemical properties as well. Superalloys are usually based on 8A elements [2].

These alloys are designed to endure temperatures ranging from approximately 500°Cto 1400°Cwith various production and heat treatment processes [3].

Superalloys overall are preferable alloys for highly challenging engineering applications with their high corrosion resistance, good fatigue behavior, and superior high temperature creep resistance. These properties can be differed by changing the production method, for example, casting forms of Nickel-based superalloys can be used in conditions where the creep deformation is the main concern but wrought alloys can be suitable for fatigue-limited turbine disk applications with it's relatively finer grains. It is noticeable that since they were first introduced between the 1940s and 1950's they had a tremendous effect on much ındustrial development [1].

### 2.1 Classification of Superalloys

Depending on the application there are a lot of superalloys are being used in different industries. Main industries for superalloy applications are mostly required, high-temperature strength and surface stability which can be exemplified as; aero-engine

industries, power plantations, nuclear-powering industries, chemical plants, etc.4 With changing the applications site and operating conditions such as temperature and aggressively of the ambient where the part will be operating, superalloys can be found in different forms as shown in down below;

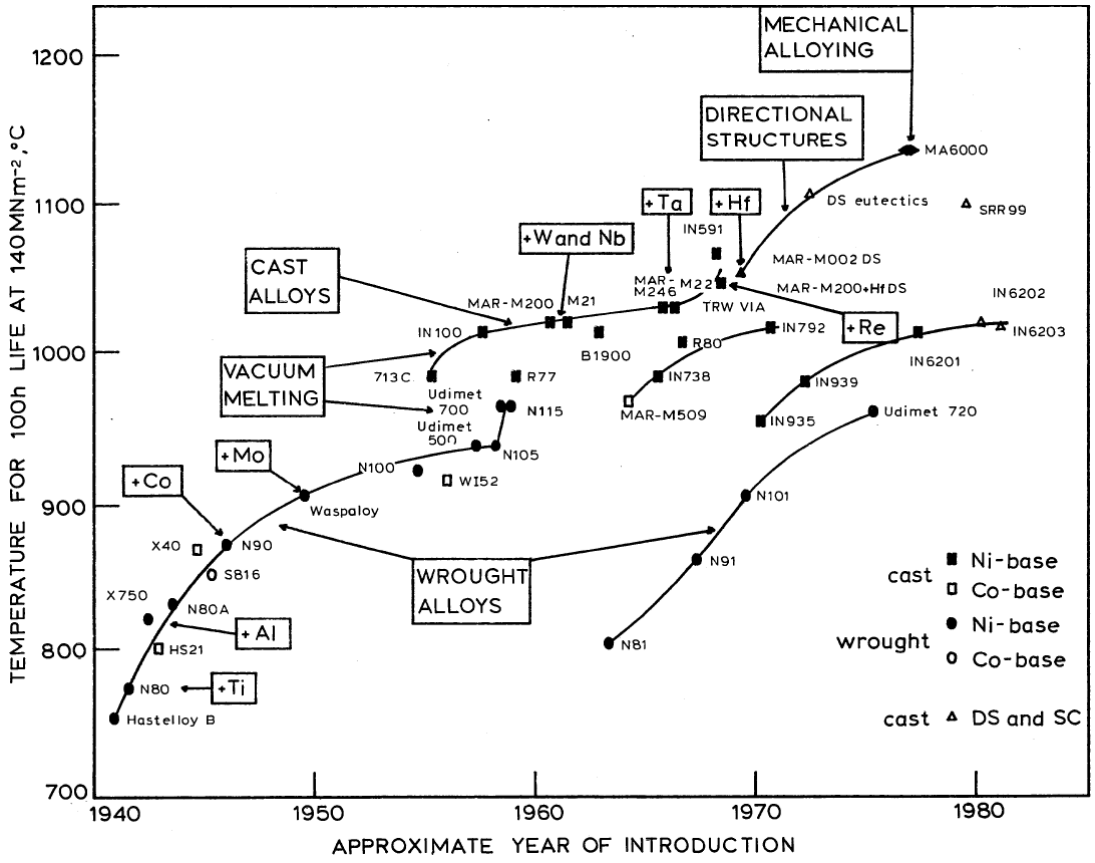


**Figure 2.1 :** Temperature capability of alloys versus year of introduction; DS directional solidified, SC single crystal [4].

Modern superalloys can consist of up to 15 alloying elements depending on their operating needs. However, superalloys can be defined in 3 main groups which are down below; [1].

i. Nickel based

ii. Iron-Nickel Based

iii. Cobalt Based

**Table 2.1 :** Influences of the alloying elements on superalloy [5].

| Influence | Alloying Elements | | | | | | | | | | | |
|---|---|---|---|---|---|---|---|---|---|---|---|---|
| | Cr | Al | Ti | Co | Mo | W | B | Zr | C | Nb | Hf | Ta |
| Matrix Strenghtening | × | | | × | × | × | | | | | | |
| γ'-formers | | × | × | | | | | | | × | | × |
| Carbide-Formers | × | | × | | × | × | | | | × | × | × |
| Grain Boundary Strengthening | | | | | | | × | × | × | | × | |
| Oxide scale formers | × | × | | | | | | | | | | |

Apart from the selected elements, these alloys may undergo different strengthening processes to increase the resistance of the material to ambient conditions. These processes can be summarised like down below;

i. Solid Solution Strengthening;

ii. Superalloys contain a lot of different sized elements which may sit on the matrix lattices, this changes lattices behavior under loading causing strengthening.

iii. Precipitation Strengthening;

iv. Superalloys contain a form of precipitations which are based on the main element with high mount added alloying elements like Ti, Al. These precipitates with solid solutionized lattices create an unfavorable environment for dislocation movement.

v. Coherency Strengthening;

vi. The difference in matrix lattices and precipitate lattices creates lattice misfits between each other which causes an impending effect on dislocation motion.

vii. Grain boundary Strengthening;

viii. High energy zones like grain boundaries can impend dislocation motion.

Besides these four strengthening mechanisms for some applications or some specific needs (creep, fatigue, etc.) some of them may not be suitable however precipitation hardening method is widely used in superalloy production [6].

Various strengthening methods can be implemented to superalloys manufacturing, besides form strengthening methods also material form selection is important to meet operating condition needs. Depending on their application, superalloys can be found in form as; bar, forging(wrought), cast, directionally solidified, single crystal, 3 dimensional printed, etc.

## 2.2 Superalloy Inconel718

**Table 2.2 :** Approximate elemental composition of the Inconel 718 Alloy [5].

| Alloy | Composition (wt%) of elements | | | | | | | | | |
|---|---|---|---|---|---|---|---|---|---|---|
| | Ni | Cr | Co | Ti | Al | Mo | C | Zr | B | Fe | Nb |
| Inconel718 | Balance | 19 | 3 | 0.9 | 0.6 | 3 | 0.04 | N/A | N/A | 20 | 5.2 |

Nickel superalloys are widely used as a turbine material in aerospace engines. As shown in Figure 2.2 with increasing temperature which means increasing the engine efficiency Nickel-based superalloys come forward to meet high-temperature requirements. Applications include both discs and blades, initially, produced Ni based for these applications are Inconel 718 and Inconel 901. These early applications need have met by conventional casting ingots, forged billets, forged discs routes, etc. Since these first applications, Inconel 718 is still one of the most common used alloy in engine application with its newly improved production methods [5].

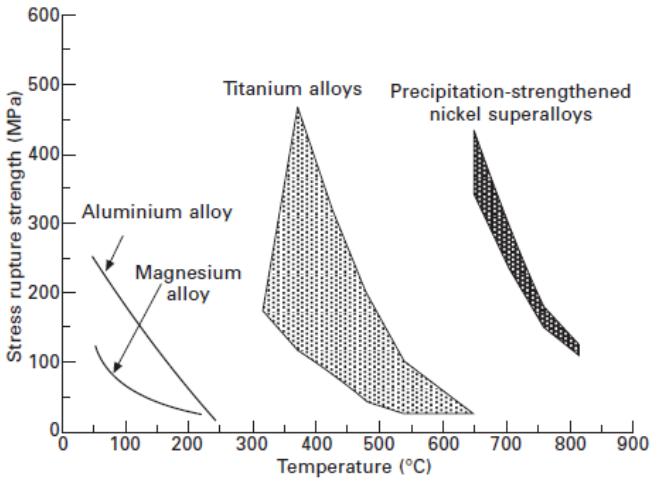


**Figure 2.2 :** Stress Rupture Strenght comparison in different temperatures between different alloy types [7].

Nickel is in the 5th place in terms of element abundance in the earth, has a face-centered cubic crystal structure (FCC) which is closed packed lattice causing high resistance to displacement movement. As mentioned in table 2.2 Fe, Ti, Al can be considered as the main alloying elements in Nickel superalloys. With these and other elements in nickel alloys, phase forms are briefly down below;

- The gamma phase (γ): Base phase usually contains Co, Cr, Mo, Ru, Re, Fe with Ni main element. This phase has an FCC structure.

- Gamma prime (γ′): Intermetallic precipitate phase coherent with matrix phase, main strengthening phase has FCC structure. Contains Ni, Al, Ti $Ni_3$(Al, Ti)
- Gamma double prime (γ″): Coherent but metastable state precipitate with body-centered tetragonal (BCT) structure. The main strengthening precipitate of Ni-Fe superalloys consist of Nb; Ni3Nb, with increasing temperature stability of this phase, decreases and tend to transform to delta (δ) phase.
- Delta phase (δ): Precipitate usually presents along the grain boundaries. These precipitates do not have an increasing effect on strengthening and have a decreasing effect because of depletion of (γ″), however can increase the grain boundary sliding resistance which improves creep resistance. Has an orthorhombic structure. Mainly composed by Ni, Ti, Nb
- Carbides and borides: Usually present at grain boundaries and increase creep-rupture resistance of superalloys. Carbide formation occurs with a Carbon reaction with elements such as Cr, Mo, Ti, Ta, Hf and creates MC molecules. Borides present in superalloys grain boundaries in form of tetragonal unit celled M3B2 [8].

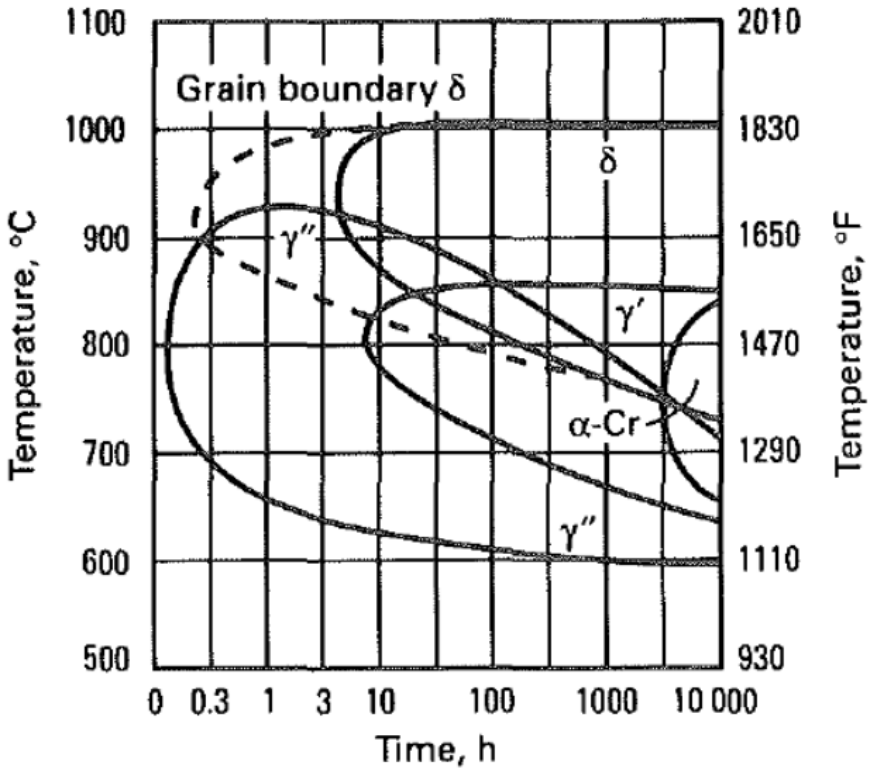


**Figure 2.3 :** Time Temperature Transformation diagram of Inconel 718 [9].

## 2.3 Superalloy Inconel718 Forged Bar;

In the aerospace industry, a wide range of material types can be used according to operation needs as mentioned in previous chapters. These different operation conditions and requirements can be met by changing the form of the material product rather than changing the material itself.

In gas turbine engines metallic materials can be manufactured from various production methods which can be summarised by; sheets, bars, forgings, additive manufactured parts, castings, etc. These material forms can be preferred according to certain operation missions such as casings, disks, shafts, etc.

The first usage of the Inconel 718 alloy in the aerospace industry starts with Saturn/Apollo programs. Showing high resistance to stress relief crackling in comparison with Waspaloy and Rene-41 made this material more preferable. The first mission to meet their needs was injector back-plate, fuel pump second stage turbine disks can be given as examples.

In this work forged bar form of Inconel 718 has been used because of it is wide usage from the gearbox, shaft materials to aviation bolts and nuts.[10] After forging process of Inconel718 heat treatments according to AMS5663 is applied to the material and after heat treatment observed initial microstructure, mechanical and physical properties are down below;

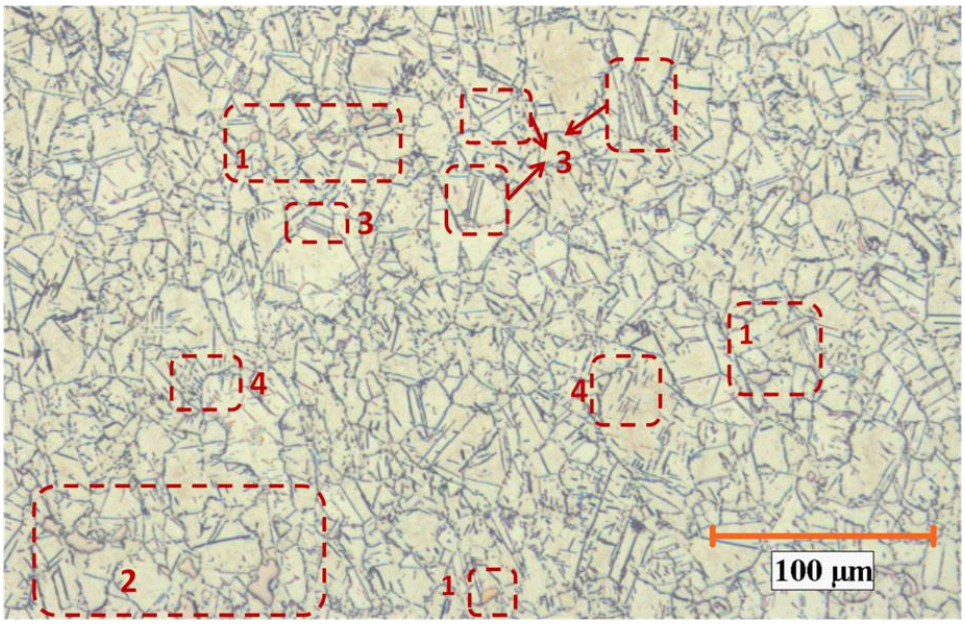


**Figure 2.4 :** Initial microstructre of Inconel718 under 200x magnification shoving; 1)Ti rich carbonitride, 2) Nb rich carbonitride, 3) Twinnings, 4) Delta phase.

**Table 2.3 :** Mechanical Properties of Inconel 718 AMS 5663 Material [11].

| Temperature (◦F)<br>Property | Grain Direction | Room Temperture | 1200 (◦F) |
|---|---|---|---|
| Tensile Stress(ksi) | Longitudial | 185 | 145 |
| | Long Transverse for forging | 180 | 140 |
| | Transverse for Bars | 180 | 140 |
| Yied Strenth (0.2% offset),ksi | Longitudial<br>Long Transverse for forging<br>Transverse for Bars | 150 | 125 |
| Elongation in 2 in.% | Longitudial | 12 | 12 |
| | Long Transverse for forging | 10 | 10 |
| | Transverse for Bars | 6 | 6 |
| Reduction of area % | Longitudial | 15 | 15 |
| | Long Transverse for forging | 12 | 12 |
| | Transverse for Bars | 8 | 8 |
| Hardness | - | 331 BHN | - |

**Table 2.4 :** Physical Constanst of the material [11].

| Pysical Constants | | |
|---|---|---|
| Density lb/in3 | Annealed | 0.296 |
| | Annealed and aged | 0.297 |
| Melting range | °C | 1260-1336 |
| Specific heat | (at 21°C, J/kg °C) | 435 |
| Curie temperature °C | Annealed | <-196 |
| | Annealed and aged | -112 |

**Table 2.5 :** Modulus of Elasticity and Shear behavior of Inconel 718 (data has been generated from hot rolled flat heat trated 1800F/1 hr+ air cooling+ 1325F/8hr+controlled cooling with 20F/hr to 1150F total aging hours of 18 hr.) [11].

| Temperature °C | Young Modulus Gpa | Shear Modulus Gpa | Poissons Ratio |
|---|---|---|---|
| 21 | 199.9 | 77.2 | 0.294 |
| 149 | 193 | 75.1 | 0.28 |
| 204 | 190.3 | 74.5 | 0.28 |
| 260 | 186.8 | 73.1 | 0.275 |
| 316 | 184.1 | 72.4 | 0.272 |
| 371 | 180.6 | 71 | 0.273 |
| 427 | 177.9 | 69.6 | 0.271 |
| 482 | 174.4 | 68.3 | 0.272 |
| 593 | 166.8 | 65.5 | 0.276 |
| 649 | 163.4 | 63.4 | 0.283 |

## 3. FATIGUE CALCULATIONS WITH STATISTICAL APPROACHES

Developments in mechanical, civil, aerospace engineering have led to new design perspectives to come up. And these new requirements also forced material science to thrive in terms of material classification. Using classification usually, refers to a material's chemical and physical properties however for certain mission materials have to classify and understood in terms of that mission needs, for example, creep, fatigue, corrosion, etc. For that purpose new testing methods were developed such as deadweight creep tests, rotating bending fatigue tests, axial fatigue tests, thermomechanical fatigue tests, etc. In the late 19th century one of the first approaches for these phenomena Mr. Wöhler stated;"Rupture may be caused, not only by a steady load which exceeds the carrying strength but also by repeated application of stresses, none of which are equal to this carrying strength. The differences of these stresses are measures of the disturbance of the continuity, in so far as by their increase the minimum stress which is still necessary for rupture diminishes"[12].

This new approach formed the foundation stones of the new design perspective, nowadays for designing certain industrial parts fatigue is one of the key criteria. In brief, the explanation as Mr.Wöhler stated, fatigue is the phenomenon where the permanent deformation is caused by continuing application of force to the material.

### 3.1 Fatigue Testing;

Design approaches have changed in many ways since the beginning of industrial development in human history. As mentioned in previous chapters increasing demanding industrial designs also led to a development in material characterization systems. The material characterization can be related to a lot of perspectives such as chemical, physical and mechanical. In terms of mechanical characterization often aiming to understand static properties comes forward. After developments in static testings, dynamic behavior characterization needs to have occurred with increasing industrial demands.

First recorded fatigue phenomena have come up in the mining industry Wilhelm August Julius Albert who is a German mining administrator observed and reported failure of mine hoist cables caused by repeated small loadings in 1829. Like this example another early reportings of fatigue had observed in the railway industry, in 1840 William John Macquorn Rankine have reported progressive brittle crack growth in railway axles.

Until the 1860's fatigue phenomena in engineering applications have only been reported and little amount experimental Works have performed, in 1861

With the request of the UK parliament, William Fairbairn has developed experiments on boilers, mills, bridges, etc showing the load level which can not deform material statically yet can create catastrophic failure on the material.

Early Works on fatigue can be summarised by specific part experiments which are only defined for certain applications and geometry. Subsequent experimental works cause more standardized tests. In 1870 August Wöhler German engineer summarised his Works again in railroad axles and concluded the cyclic stress range is much more important than peak loads and firstly introduced the perspective of endurance (fatigue) limit and introduced the Wöhler curve. Further his Works led to developments in steel and iron cyclic testing methods which broke new ground in terms of testing methodologies.

After these experimental Works developments in understanding fatigue and testing, methodology increased rapidly, in 1910 O.H Basquin showed a linear relationship over a wide stress range in log base is still used today, the relation is given in formula 3.1. Where "C" and "b" are empirical constants that define power-law relation. "b" can be expressed as slope and "C" is the intercept. Like this development fallowing developments achieved in the 20th century; Minors rule (1945), Coffin-Manson (1954), Erdoğan-Gomez-Paris (1961), Rain Flow Counting Algorithm (1968).

$$C = \Delta\sigma N f^{b} \tag{3.1}$$

Enhancements in testing approaches and testing systems led to create alternatives for specific part test in terms of obtain fail safe desing. With advanced computing and analyzing systems designing processes can be integrated to specimen type more standardised tests.

Fatigue test can be roughly divided with certain factors which are down below;

**Table 3.1 :** Possible distinctive features of fatigue testing.

| Loading Condition | Loading Type | Temperature Gradient | Specimen Type | Control Mode |
|---|---|---|---|---|
| Variable Amplitude | Axial | Isothermal | Actual Part | Displacement |
| Constant Amplitude | Alternating Torsion | Cyclic Heating and Cooling | Semi product | Applied Force |
| Constant Amplitude With holding at peak/valleys | Plane Bending | | Standart Specimen | Material Unit Strain |
| | Rotating Beam Bending | | | |
| | Combined Stress | | | |

Discoveries in engineering led to a standardization of material testing and in terms of that enterprises formed over the last century such as; ASTM, ISO, MMPDS, NADCAP, etc. These enterprises aim to standardize the designing procedures, quality of work done, and increasing the repeatability of the work. Some of the standard examples are down below;

**Table 3.2 :** Examples standards relating fatigue testing.

| Standard Code | Standard Name | Organisation |
|---|---|---|
| ASTM E606 | Standard Test Method For Strain-Controlled Fatigue Testing | American Society for Testing and Materials |
| ASTM E466 | Standard Test Method For Force-Controlled Fatigue Testing | American Society for Testing and Materials |
| ASTM E647 | Standard Test Metho For Measurement of Fatigue Crack Growth Rates | American Society for Testing and Materials |
| ISO/DIS 22407 | Axial Plane Bending Method | International Organization Of Standardization |
| ISO 12108 | Fatigue Crack Growth Method | International Organization Of Standardization |
| ISO 1099 | Axial Force Controlled Method | International Organization Of Standardization |
| ISO 12106 | Axial Strain Controlled Method | International Organization Of Standardization |
| ASTM STP1231 | The Significance Of Variable Amplitude Fatigue Testing | American Society for Testing and Materials |

Under these standard methods, during the fatigue tests load cycle relation can be schematically illustrated down below;

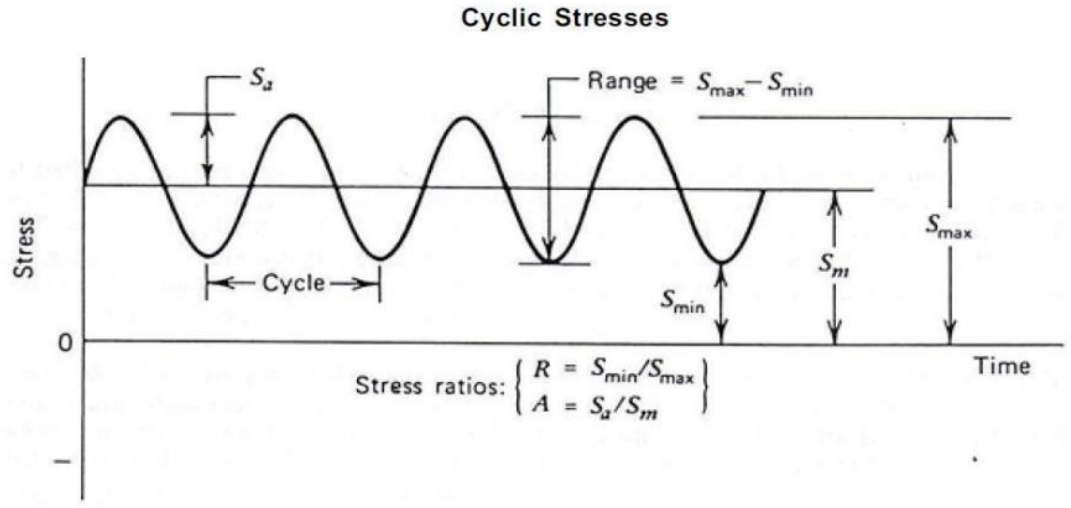


**Figure 3.1 :** Illustration of fatigue constant amplitude cycling [13].

From this illustration down below terms shall be defined as;

Peak Stress/Strain(Smax): Maximum applied Stres sor Strain depending on the test type

Valley Stress/Strain(Smin): Minimum applied Stres sor Strain depending on the test type

Mean Stress/Strain(Sm)= Value is to define the stres or strain level where the peak to mean and valley to mean differences are equal

Stres sor Strain R ratio(R): Is the value definin ratio between peak and valley value.

Amplitude/alternating Stress/strain(Sa): Distance between the mean to peak or mean to valley.

Stress /Strain A ratio: Ratio between alternating and mean value

Cycle: Containing 2 loading and unloading sections in unit time.

Stress/ Strain Range(Sr): Distance between peak and valley value.

Combined formulation of fatigue paremeters are given in equation 3.2.

$$R = \frac{Smin}{Smax} \quad A = \frac{Sa}{Sm} \quad Sa = \frac{Smax - Smin}{2} \quad Sr = Smax - Smin \tag{3.2}$$

As stated in the exampled fatigue standards, fatigue tests can be performed under different control modes such as; force (stress) and strain. These different control modes are applied to provide cyclic behavior data for different design approaches. Here high cycle fatigue and low cycle fatigue come forward. These two terms differ

from the two different fatigue testing concepts with their counted cycle values. However, these two fatigue tests differ themselves with their testing conditions which are down below;

**Table 3.3 :** LCF/HCF Comparison table.

| Name | Range/ Discription | |
|---|---|---|
| | **LCF** | **HCF** |
| Loading condition | Axial | Axial |
| Stress levels | Above Yield Point | Below Yield Point |
| Cycle ranges approximately | <10^5 | >10^5 |
| Related Standard | ASTM E606 | ASTM E466 |
| Fracture evaluation | Relatively longer crack propagation duration | Relatively shorter crack growth and sudden fracture |
| Fracture surface | Relatively wider crack growth zones | Relatively narrower crack growth zones |

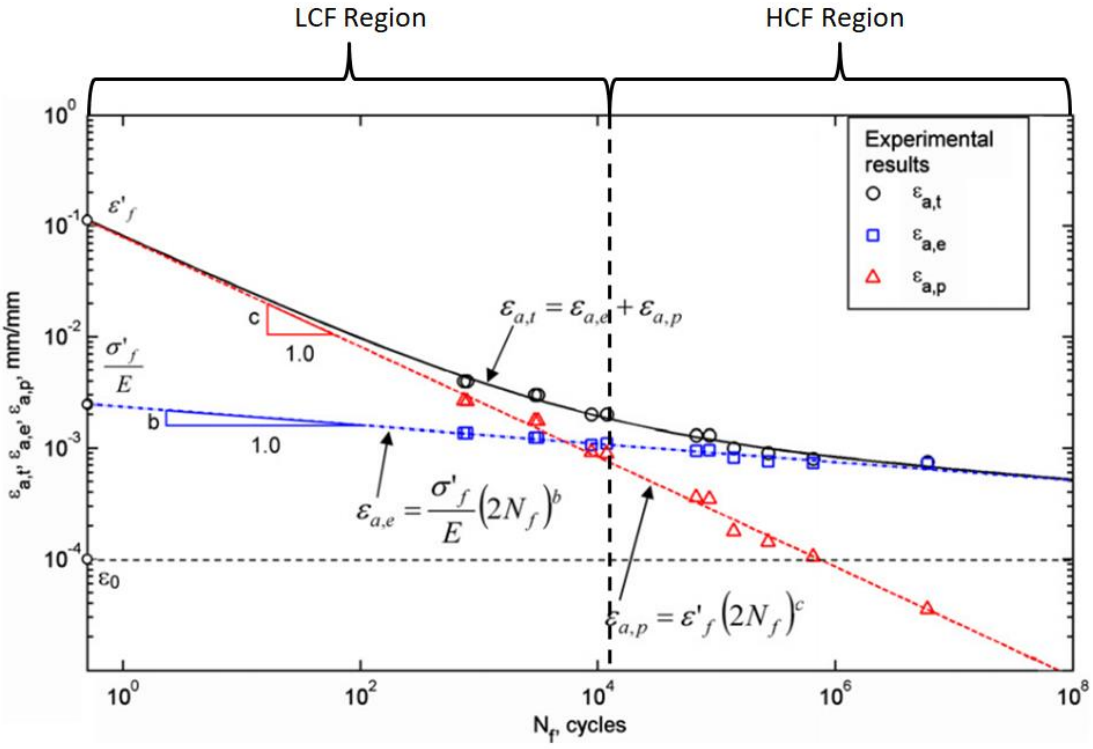


**Figure 3.2 :** Example of the Manson-Coffin-Basquin with showing approximate LCF-HCF regions [14].

These 2 fatigue testing approaches can be performed to define materials cyclic behavior under different conditions. Apart from that in terms of fatigue design, different sorts of factors have to be considered to define materials behavior which is down below;

- Type of the loading
- Component size and stress/strain distribution
- Surface conditions and directional properties
- Stress/Strain concentrations
- Mean stress/strain
- Environmental effects(corrosion)
- Metallurgical Factors
- Loading/straining rate, frequency effect [15].

In terms of understanding material fatigue behavior and creating designs, standard fatigue tests are always helpful. As mentioned above depending on the design requirement some parts require more plastically endurance yet some of them only require elastic durability for that part design. With an aiming elastic endurance perspective, the term endurance limit comes forward. Endurance Limit is the term that defines material behavior for a certain cycle limit. Depending on the material properties and industrial application endurance limit can be exampled as stress level where the fatigue life lasts longer than or equal to 10^7 cycles.

The concept of endurance limit is highly dependent on industrial needs in the first place. In the past half-decade with developments in testing technologies fatigue tests performed under resonance type testing machines or ultrasonic testing machines reaching frequency levels from 80Hz to 20kHz aiming to reach cycle values >10^8 to 10^10. With reaching these cycle values new terms such as Giga-cycle fatigue and very high cycle fatigue came up. As mentioned in previous chapters, fatigue failure is normally expected at the material surface but in this case of reaching 10^9-10^10 cycles, researchers observed that interior fracture initiation becomes the dominant fracture mechanism.[12] Between commonly defined fatigue life ranges normally failure mechanism can be summarised as surface crack initiation or crack initiation from inner discontinuities such as inclusions, defects, etc. On the other hand, fatigue cycles which are exceeded the common ranges present more inner crack initiations mostly along with the material slip bands.

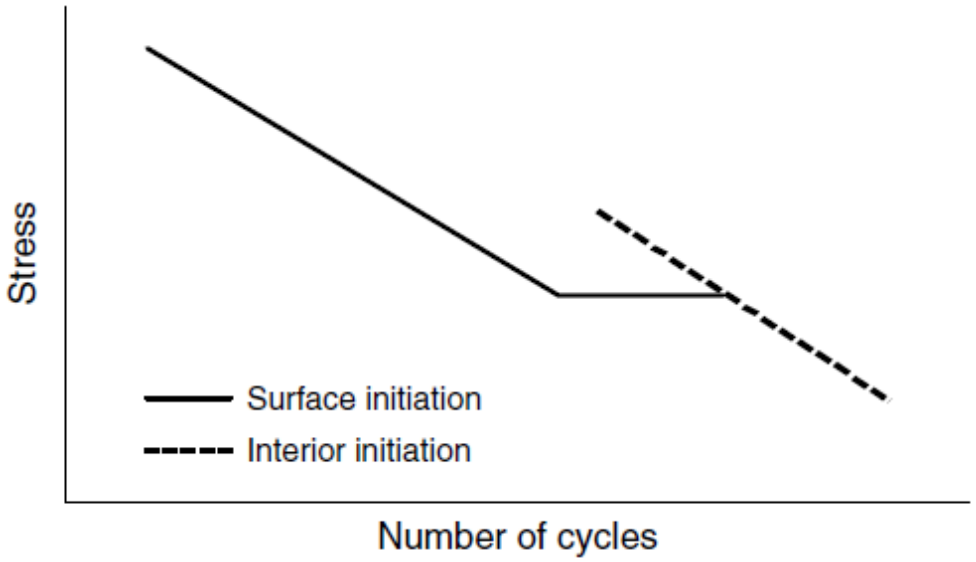


**Figure 3.3 :** Schematically presenting changing the trend of the fatigue data [12].

Material testing is crucial in terms of starting the design of a new part, however, it is unrealistic to expect the actual part to show the same behavior under cyclic loading. To predict that certain approaches can be used.

For example, modifying the accepted endurance limit or modifying the Wöhler curve can be an option. For modifying the endurance limit equation down below can be used, the coefficients used in this calculation are all empirical yet can be calculated according to some acceptance, given in equation 3.3 [16].

$$Se = ka \times kb \times kc \times kd \times ke \times kf \times S'e \tag{3.3}$$

ka= Surface condition factor, kb= size factor ,kc=loading condition, kd=temperature factor, ke=reliability factor, kf=miscellaneous effects, S'e=Test specimen endurance limit, Se=Endurance limit at the critical location of a machine part in the geometry and condition of use

$$ka = a \times Sut^{b} \tag{3.4}$$

**Table 3.4 :** Coefficiet discription for ka factor calculation [16].

| For ka factor | | |
|---|---|---|
| Surface Finish | Factor a(mpa) | Exponent b |
| Ground | 1.58 | -0.085 |
| Machined cold drawn | 4.51 | -0.265 |
| Hot-rolled | 57.7 | -0.718 |
| As Forged | 272 | -0.995 |

### 3.2 Rotating Bending fatigue tests;

There are a lot of different testing machines for different material testing methods in various industries. As mentioned previous chapter in fatigue testing, there are different types of testing systems according to load application. Different loading applications and test control methods also require a different types of testing devices and testing designs. For axial tests with both stress-controlled and strain-controlled servo-hydraulic testing systems are widely used. Electromechanical testing systems can be used also for axial tests depending on industrial needs. However, these testing systems are often expensive and relatively slow in terms of generating fatigue test data.

Rotating bending testing systems are relatively cheap and fast with using an electrical motor for rotating the specimen. There are different types of rotating bending test machines according to their load application ways. Deadweight Rotating bending testing systems are more widely used because of their relatively low expenses.

The test is performed with electrical motor excitation to rotate the support bearings to load bearings which will transfer the rotation to the specimen. Loading is performed by hanging the load plates to load bearings which will also create a bending moment on the specimen.

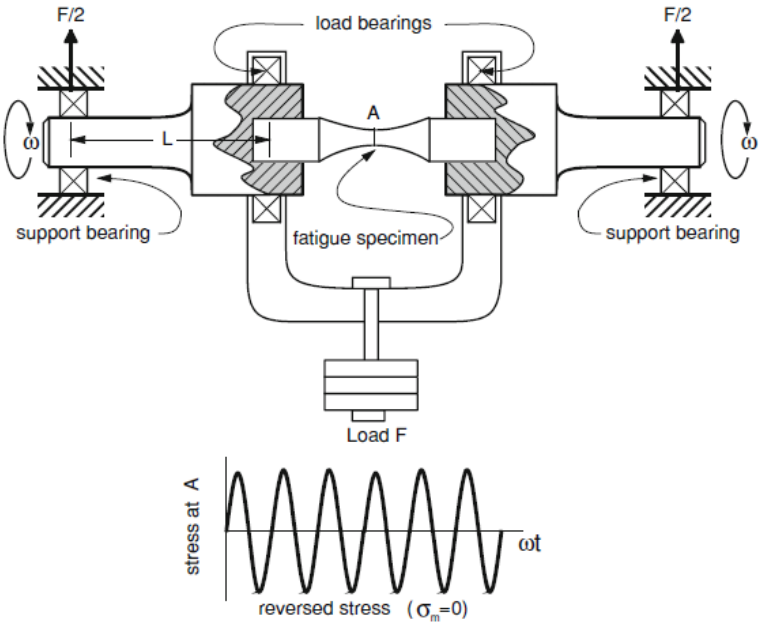


**Figure 3.4 :** Schematical discription of rotation bending testing system [17].

The rotating bending test is a load-controlled test as mentioned in previous paragraphs. Stress is calculated using loading moment and moment of inertia which is depending on the specimen geometry.

$$\sigma = \frac{32M}{\pi d\text{^}3} \tag{3.5}$$

Where the M is moment and equals to :

$$M = F \times L \tag{3.6}$$

Where F is the applied force and the L is the distance to moment arm.

### 3.3 Determination of Fatigue Behavior And Statistical Approaches

Material tests are performed in order to describe material behavior under certain conditions. However, these tests are only a tool to understand the mechanisms, to make comments, and perform design approaches statistical methods are used. There are various different methods for different observed populations and distributions.

Statistical methods for these observations start with best-fit calculations. Best fit model equations can vary, different mathematical equations can be used as soon as desired data is calculated. According to population distributions different model equations can be used, linear relationships are widely used, alternatively polynomial and logarithmic equations can be used too.

**Table 3.5 :** Different applicable model equations.

| Model | Equation |
|---|---|
| Basquin[12] | $C = \Delta\sigma \times Nf^{b}$ |
| Exponential | $\sigma = a \times e^{(\log Nf \times b)}$ |
| Mansons Equal Slopes[19] | $\Delta\varepsilon = (\frac{a \times \sigma B}{E} \times Nf^{b}) + (\varepsilon f^{c} \times Nf^{d})$ |
| ASTM E739 Linear Fitting[20] | $Y = A + BX$ |

*Note: a,A,b,B,c,C,d are stands for estimators, σ=Applied stress, Δσ=Applied stress range, σB=Tensile stress, E=modulus of elasticity, Nf=Cycles to failure, Δε=Principal strain range, εf=true fracture strain under axial loading*

In Table 3.5 example model equations that are used in this work are given. Model equation's common feature is they all include fitting estimators which can be calculated with iterative solving systems, given as an individual letter in equations. To calculate these estimators one of the widely used and relatively easy ones is least squares regression. For fatigue applications common approach is a simple linear regression model, in model singular regressor "X" has a relation with answer "Y" which is close to straight line.[21] Applied regression aims to minimize the summation of squared residuals, estimators which are minimizes this result can be accepted as appropriate.

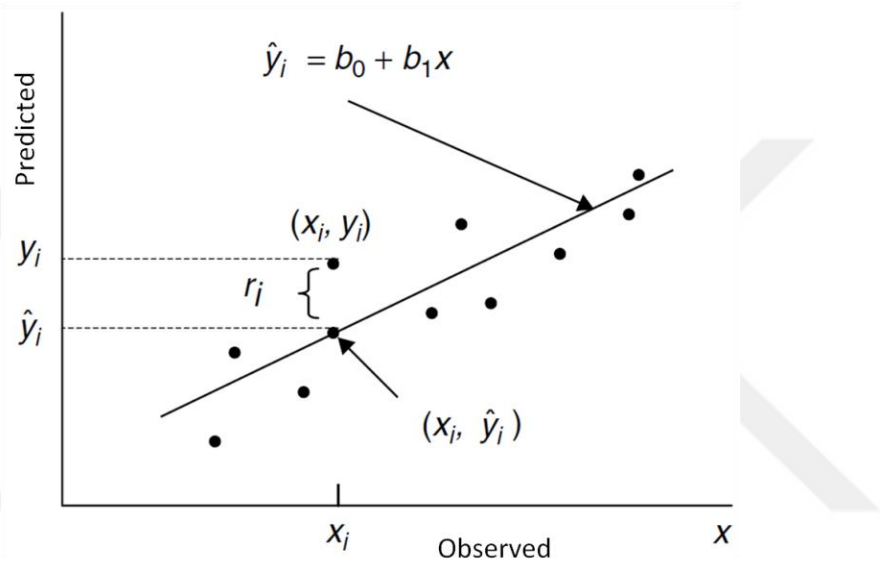


**Figure 3.5 :** Description of Least Square analysis,r = residual, y = calculated values,, x = observed values, and linear relationship between them [22].

Residual values can be calculated easily by subtracting the calculated data from observed data for each predictor. According to the observed population, different regressions can be implemented too. In the case where observations mostly exceed the testing limit or certain data exceeds the testing limit, maximum likelihood regression can be used. The difference between least squares and maximum likelihood is in the least-squares regression all observations are accepted as failed for example if the life testing has a certain time limit to terminate the test while analyzing the data with least squares the data that has been exceeded the test time limit will be considered as failed data, but in maximum likelihood model, regression estimates approximated failure point for these kinds of data. In this case, the selection may differ according to the engineering design, if the design is more life-critical least squares regression will be relatively safer. In the figure down below description of Maximum likelihood, regression is given. Unlike from least-squares maximum likelihood regression model

aims to maximize the defined likelihood function. [23] As can be seen below figure Maximum Likelihood estimation aims to define the most favorable point to describe population according to its deviation.

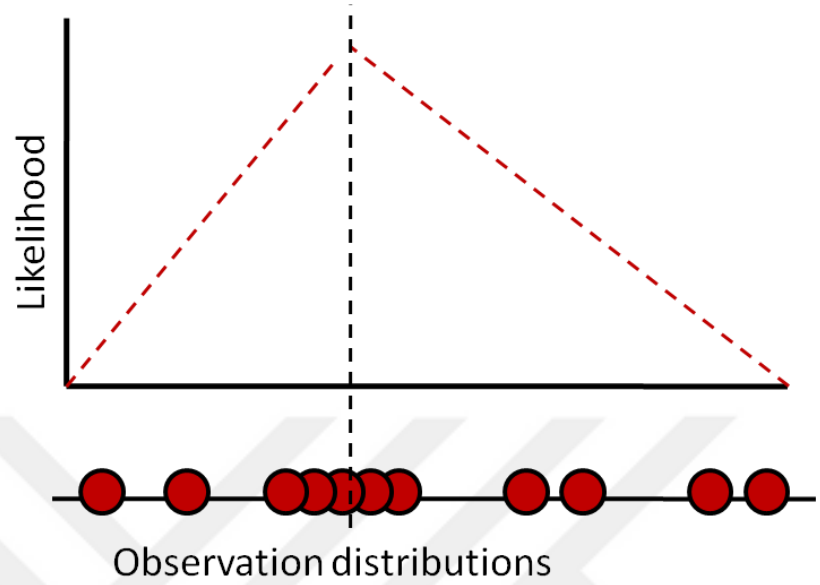


**Figure 3.6 :** Maximum Likelihood Schematically.

Explained regressions can be used with different data distributions, in terms of data distribution it is important to understand the observed population. Generally, observations are processed statistically assuming that they fit the normal distribution, however, there are lot's of different studies proving that Weibull distribution is equally or better than normal distribution in terms of calculating the best fit curve [24] [25] [26].

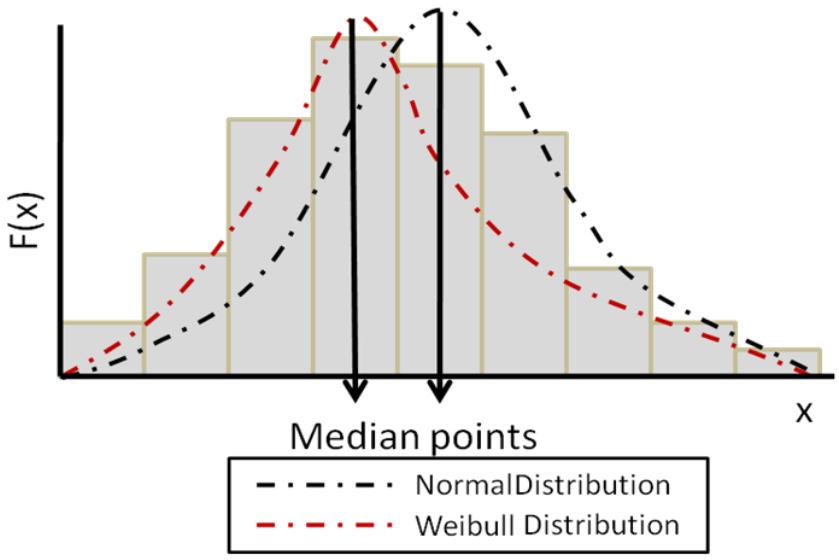


**Figure 3.7 :** Schematical description of normal and weibull distributions.

As it can be seen in the schematical description of two distributions, these two distributions are different assumptions on a certain population. In the cases where the observations tend to deviate from the arithmetic average of observed values, this means the population is skewed. For skewed populations, log-normal distribution and Weibull distribution give a more reliable approach. [27] Applicability of different distribution can be defined with different statistical tests such as Kolmogorov-Smirnov (KS) test, Anderson-Darling Test, Chi-Square Goodness of fit test. These example tests questions if a sample comes from a population with a specific distribution.[28] After calculating bet fit curves, another step should be performed is outlier analysis, there are different approaches for that such as, box-plot comparisons, studentized t distribution comparison. [29] In this work both procedures are calculated to understand the population more. For studentized t distribution, fallowing calculations should be performed; [27].

$$T_i = \frac{SR_i}{(1-h_i)^{1/2}} \times \left(\frac{RMSE}{RMSE_i}\right) SR_i = \frac{R_i}{SD} \tag{3.7}$$

$$SD = RMSE = \sqrt{\sum_{i=1}^{n} \frac{{R_i}^2}{n-k}} \tag{3.8}$$

$$h_i = \frac{X_{1i}^2\left(\sum X_{2j}^2\right) - 2X_{1i}X_{2i}\left(\sum X_{1j}X_{2j}\right) + X_{2j}^2\left(\sum X_{1j}^2\right)}{\left(\sum X_{1j}^2\right)\left(\sum X_{2j}^2\right) - \left(\sum X_{1j}X_{2j}^2\right)} \tag{3.9}$$

**Table 3.6 :** Item descriptions from equations.

| ITEM | Description |
|---|---|
| $T_i$ | Studendized t |
| $SR_i$ | Standardized residual |
| $SD$ | Standard deviation |
| $RMSE$ | Root mean square error for entire sample |
| $RMSE_i$ | RMSE for *i*th observation |
| $R_i$ | Residual |
| $n$ | Sample size |
| $k$ | Number of parameter estimated |
| $i$ | i=1 to n |
| $j$ | j=1 to n |
| $\alpha$ | Desired significance level (example; 0,05) |

After calculating studentized t distribution for each observation, critical T value has to be determined with Bonferroni Inequality that describes critical T as an upper percentile of the central t distribution with "n-k-1" degrees of freedom with desired significance level. [27] Next step is to compare each $T_i$ value with critical T value as follows;

$$A = \max[T_i] \tag{3.10}$$

$$A > t(\frac{\alpha}{2n}, n-k-1) \tag{3.11}$$

If the calculated A values ensure the requirement above that means, under this condition probability of certain data is to be an outlier is less than the given significance level. Detected outlier observations can remove from analysis however in terms of engineering applications if there are no detectable mechanical or physical reasons outlier observations can be implemented in the population to make a more conservative approach. Calculated best fit curves should be investigated in order to understand how the best-fit curve complies with the observation data. To do that two widely used methods can be used. The first one is calculating the coefficient of determination also known as $R^2$. Coefficient of determination has a value between, relatively good fitted curve converges to. That means variability which is observed through the population in "y" is explained by the regression model.

$$SS_{res} = \sum_{i=1}^{n} {R_i}^2 \quad SS_{tot} = \sum_{i=1}^{n} (y_i - \overline{y})^2 \quad R^2 = \left(1 - \frac{SS_{res}}{SS_{tot}}\right) \tag{3.12}$$

$SS_{res}$ stands for the measurement of the variability in y, $SS_{tot}$ stands for the measurement of the variability in y without counting in to account of regressor variable x. "y" is in our case is observed life values [27].

Last but not least, after determining the coefficient of determination, a lack of fit test should be implemented. One of the most common lack of fit test methods is Durbin Watson Test. Durbin and Watson documented this test in 1950 first and additional studies are performed from 1951 to 1971 [27] To do this test fallowing calculations is performed;

$$D_i = \frac{\sum_{i=2}^{n} (SR_i - SR_{i-1})^2}{\sum_{i=1}^{n} SR_i^2} \tag{3.13}$$

$$Dc < 2 - \frac{4.73}{n^{0.555}} \tag{3.14}$$

If the Di is smaller than Dc it means that there is a lack of fit, also meaning that there is a varying difference between standardized residuals of each observed data. Otherwise, the calculated best fit can be considered as sufficiently representing the observed population.

These processes are used to generate best-fit curves also known as median curves. The design likewise median curves are considered as %50 probability curves. In terms of the safe design approach, confidence intervals shall be calculated. With calculating the confidence bands median curves are used to generate maximum and minimum curves by taking into account of variance of a population. After calculating variance, according to the desired probability with using chi-squared or t distribution and according to population size Fpvalue can be selected. With this Fp value calculation down below can be used to generate confidence band curves. From Table.3.5 linear model equation is used for example;

$$X = \frac{(Y - A)}{B} \mp (F_P \times \varphi) \tag{3.15}$$

Using this equation will generate conservative curve for observed population. In equation" $\varphi$" stands for variance of population. This can be calculated as standard deviation, standard error of estimation, population standard deviation and so on.

## 4. LITERATURE SURVEY

There is an increase in the need for dynamic material property descriptions under different test conditions to meet design needs. In the early stage of advanced design practices, fatigue testing and dynamic approaches are well studied. More advanced designs and working conditions induced new testing approaches in fatigue works. Different fatigue testing studies include different temperatures than ambient temperature, different control modes (strain, load), different loading conditions (bending, axial, torsion, etc.), and so on. After developments on fatigue testing, crack propagation testing and linear elastic fracture mechanics comes up, to understand dynamic behavior more deeply. Different engineering applications require different testing conditions, to meet that need unorthodox test approaches such as multi-axial fatigue, variable amplitude loadings, sustained peak/valley loadings, thermomechanical fatigue testing are brought to fatigue studies agenda as well. Besides advancements in testing approaches fatigue test is divided into two different subgroups which are strain controlled low cycle fatigue (LCF) and load controlled high cycle fatigue (HCF).

Some of the engineering approaches are dedicated to LCF life in its design and in some cases HCF is crucial. For example, In the 1990s HCF behavior of the turbine parts are becoming a crisis in USAF for F16 and F15 fighter jets. According to a study of USAF(Air force) and USN(Navy), 40% to %50 of failures are detected from high cycle fatigue. These failures are detected mainly rotating air seals of F16, low-pressure turbine blades F15E and with further failure analysis compressor fans were also observed to failed from HCF conditions. Integrated High-Performance Turbine Engine Technology (IHPTE) program has been developed to understand and maintain a more safe design approach, which is gradually funded from $230 million to $600 million. And eventually in the early years of 2000 with the development of the F35 fighter platform Rolls-Royce Plc has joined the common initiative. In these works HCF testing, tooling, and new design approaches are worked intensively[12] In this thesis unlike widespread academic works dwell applications are integrated into rotating

bending fatigue testing aiming to understand sustained load effects to materials bending fatigue behavior.

For engine applications, recent literature works are mainly focusing on crack propagation tests under different loading conditions and dwell applications. Dwell applications are used to simulate the engine's start-stop cycles. [31] As it can be seen in Figure 4.1 in addition cyclic loading materials are subjected to variable loadings and sustained loadings as well. These variable loadings can be in form of torsion, axial or pure bending regarding the working condition of a specific part. Different loadings will have different effects on material and consequently will affect the fracture mechanics. In Figure 4.4 **s**tress distributions can be seen, it has to be noted that under rotating bending conditions specimen is subjected to compressive and tensile stresses at the same time. These differences in stress distribution effects fatigue life noticeably.

Different loading condition effects on fatigue life are widely studied subjects from the beginning of dynamic design perspectives. According to these works pure bending fatigue behavior of a material is nearly %30 higher than push-pull loadings.[15] These life differences are also lead the academic works to search for correlation between them, one early study which is published in 1987 performed in the USA aimed to predict bending fatigue life from axial fatigue results for 4130 steel.[32] In this work as a result LCF regions are sufficiently estimated accounting on plastic flow, however, due to the volumetric effects HCF regime is not sufficiently estimated.[32] A commonly accepted idea in this difference is; the lower volume of material is subjected to higher stresses in bending conditions however different from bending in axial loading in addition to surface all the cross-section is subjected to equally high-stress levels [32].

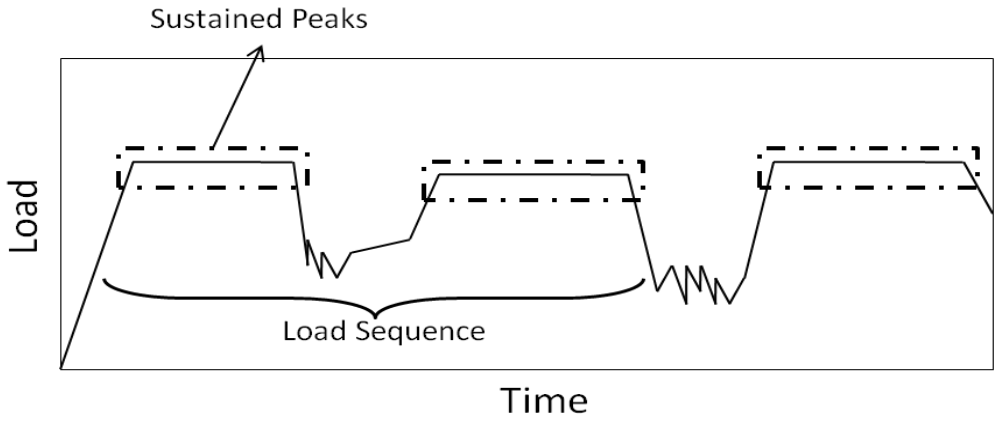


**Figure 4.1 :** Schematically description of engine load/time distribution.

Fatigue damage accumulation of smooth specimen is highly affected by dislocation movements. Even the loading levels are not as high as plastically deform the material, under cyclic loadings dislocations moves and reaches to specimen surface creating intrusions and extrusions. Which are eventually cause accumulation of stress intensity and cause crack initiation. Inconel 718 has the same behavior under cyclic loadings at room temperature and higher temperatures.[33] [34] [35] [15] Figure 4.2 shows basic description for crack ignition for smooth specimen failure.[15] This phenomena and materials cyclic response stress depends on test temperature, strain rate and applied strain amplitude.[36] Cottrell and Hull model emphasis the dislocation movements over active slip bands.

The slip band distributions and dislocations slip modes are depending on the temperature and composition of the material. The temperature change can change the activated slip bands and slip band amounts, at lower temperatures dislocations are restricted to {111} plane.[36] Increasing the temperature from ambient to relatively intermediate temperatures does not change the microstructure drastically. But increases the activated planar slip band amounts and dislocation activations.[36] In Figure 4.3**.** slip band distributions are given visibly at different temperatures for Nimonic 80A material which is also a Ni-based alloy having FCC gamma phase in the matrix.[36] From ambient temperatures to 700 $^{o}$C deformation mechanisms and dislocation movement is changes subsequently as; cross slip, by pass, diffusive.[36] Important thing is here that dislocation movement is directly dependent on stacking fault energy and Inconel 718 material has low stacking fault energy which means that it is harder to perform dislocation movements especially when dislocation comes across precipitates.[36] [37] At higher temperatures with activation of diffusion, slip bands barely visible since they are more diffusive and with that new directions can be activated such as {200}.[36] These material changes also change the material's cyclic response in terms of softening and hardening. These cyclic phenomena are widely observed in strain-controlled fatigue tests since the applied loads are relatively high means that cyclic application includes plastic deformation. In this work, these phenomena are not the main concerns since the performed test is load controlled.

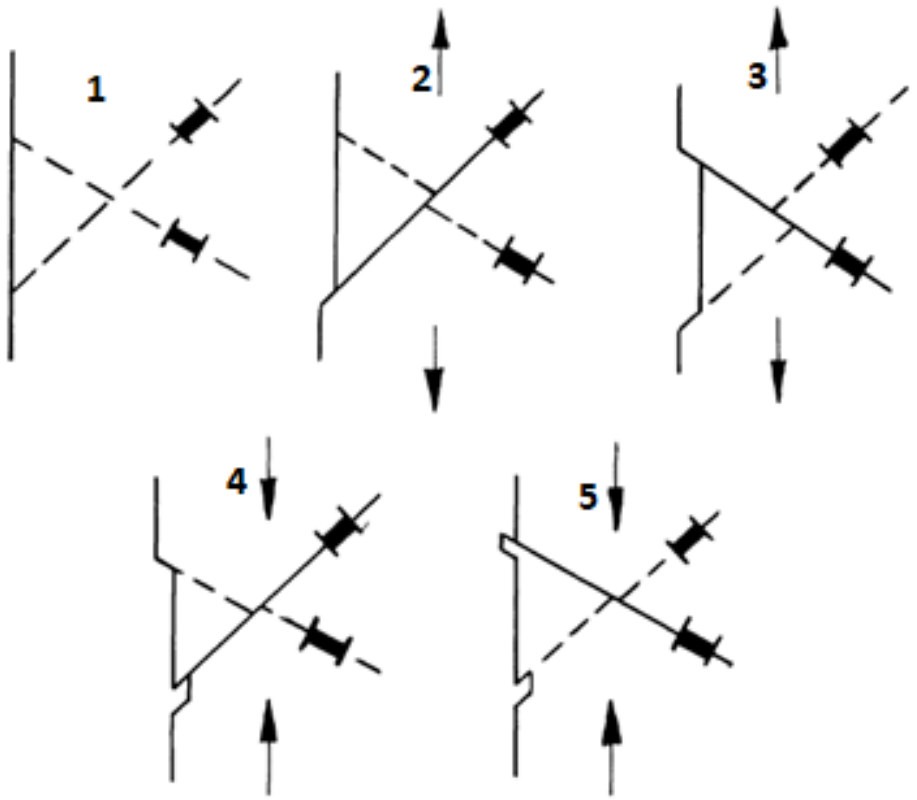


**Figure 4.2 :** Schematically description of Cottrell and Hull's model for generation of intrusions and extrusions [16].

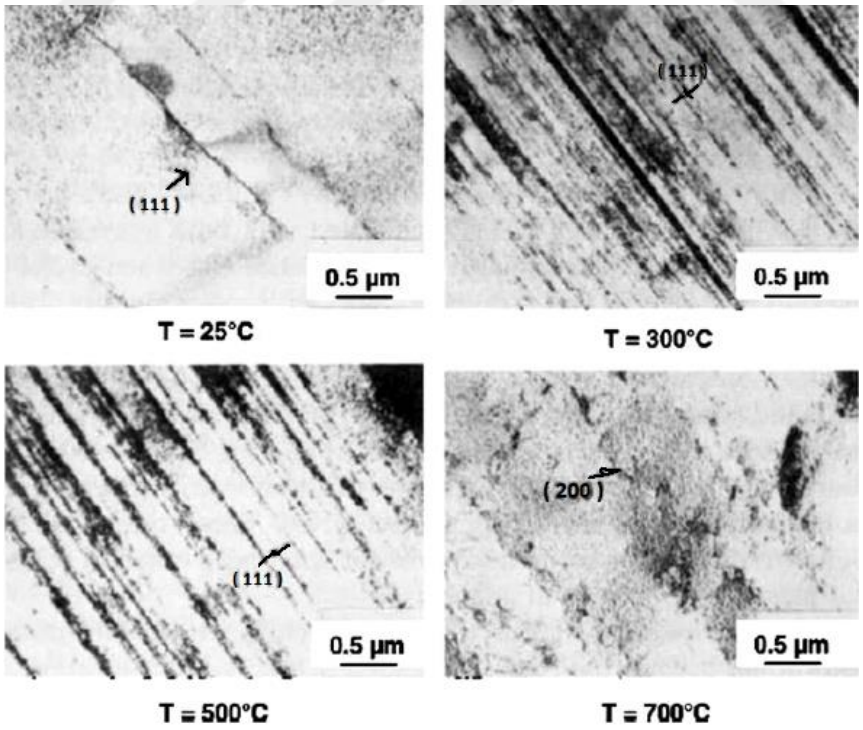


**Figure 4.3 :** Visualation of slip band distributions in different temperatures for Nimonic 80A [36].

High-cycle fatigue works in the literature include different approaches and different testing conditions. Before heading to more recent studies, In the study which is performed Idaho National Engineering Laboratory in 1991 Inconel718 material is tested under various conditions. From heat effect to dwell conditions. In this work 2 different model equations are tested in terms of curve fitting however different testing conditions also give good information about overall Inconel718 behavior. Some of the brief observations of this study are; temperature effect on life tend to decrease in HCF regime, strain rate effects observed mostly at higher temperatures, increase in grain size decreases the fatigue life, relatively at low temperatures dwell application has no visible effect and compressive dwells are more detrimental [38]. These observations are highly beneficial for developing our research targets.

One of the works which is performed at Guizhou University in 2018, emphasis the heat treatment effect on axial fatigue behavior at room temperature. Under the same testing conditions solution heat treated and aged specimens showed relatively higher life results at higher stress levels but at lower stress regions scatter is increased aged and solution heat-treated specimens showed similar results. As a result of this work difference between solution heat treated and aged specimen is approximately %6 percent. Also, it is observed that at the aged specimen under axial loading crack initiation started from multiple crack initiation sites on nonmetallic compounds [15]. Overall in here it can be stated that in aged conditions precipitates can be crucial for also strengthening but also for failure initiation.

Another study which is performed at the University of Žilina Slovakia in 2017 showed that under axial push-pull fatigue loadings life results are nearly %50 of three-point bending fatigue life, these differences are clearly seen in the endurance limit [33]. The various of testing which is studied in high cycle fatigue of Inconel718 life results are relatively deviate from one and other. This can be because of different things as different materials production heats, surface qualities, etc. However, the common observation is the crack propagation feature which is a transgranular failure. Leading more smooth fracture surface [33] [15] [12].

In the overall testing concept, it can be clearly seen that in engineering studies testing tooling and parameters evolved to observe sustained conditions, creep-fatigue interactions. In early studies besides from creep factor firstly tested condition is interruption of cyclic loading. In the study which is performed in 1972 Cambridge

University, it is observed that applying resting periods between cyclic loadings at zero load condition showed an increase in endurance limit at room temperature for steel material. This study shows an increase in life with all resting periods [39] In further work which is performed in 1983 Australia performed at higher temperatures at 300° C 4140 steel showed an increase in life as well and explaining this phenomenon is related to recovery [40]. Besides these factors under high-temperature deformation conditions, dynamic recovery is also one of the mechanisms that come to mind. Recovery and recrystallization are depended on temperature, deformation, and the material itself. Nickel alloys have low stacking fault energy which means that movements of the dislocation like; glide, cross slip, etc. are relatively hard. These two mechanisms occur under temperatures where operating temperature is above %50 of the homologous temperature of the alloy. Recovery can be also observed at lower temperatures however severe deformation or relatively high-stress application is needed.

Interruption of cyclic loading technique also used to observe the oxidation formations on the specimens during the fatigue damage. In 1999 Japan fatigue tests are performed at different temperatures using rotating bending testing. Inconel718 material was observed to increase its life by increasing the temperature in low-stress regions. The tests are performed at 300-500-600$^{o}$C and tests are interrupted and cooled down to observe surface features. In these observations, oxidation is clearly seen in the microcrack regions. According to this study, life increase is related to oxides which harden the crack nucleation. [35] Advancements in sensor technologies make it possible to perform more reliable and detailed testing. In the application of dwell and interruption cases, fatigue crack growth testing has become more and more important over the years. In a study which is performed at the University of Tennessee in 2005, generalized estimations are tabulated after examining test results of another Ni-based superalloy Hastelloy X, Haynes188-230 [41]. Expected issued which are occurs under sustained loading are tabulated in Table 4.4.

**Table 4.1 :** Possible beneficial and detrimental effects of different operating conditions [41].

| # | Testing Condition | Possible beneficial effects | Possible detrimental effects |
|---|---|---|---|
| 1 | High temperature or low frequency LCF | -Slip dispersal -Strain aging -Crack Tip Blunting -Microstructural coarsening | -Creep Damage -Environmental damage |
| 2 | Low temperature or high frequency LCF | -Elimination of creep -Elimination of environmental effects | -Increased planarity of slip |
| 3 | Tensile holds during the LCF | -Development of compressive mean stresses | -Creep damage in form of boundary cavity |
| 4 | Compressive holds during the LCF | -Sintering of the grain boundary cavities | -Development of a tensile mean stress -Initiation of cracks in the oxide scale |
| 5 | Fatigue fallowed by creep | -Cyclic work hardening | -Cyclic Work softening -Formation of crack |
| 6 | Creep fallowed by fatigue loading | -Precipitating of strengthening phases | -Little effect when grain boundary damage does not occur |
| 7 | Cyclic Creep | -Anelastic strain storage recovery | -Metallurgical recovery |

Recent studies showed that under sustained peak conditions showed an increase in fatigue crack growth dramatically. Especially at higher temperatures, two mechanisms are intensively observed; stress accelerated grain boundary oxidation (SAGBO) and dynamic embrittlement (DE). These two mechanisms depend on oxidation diffusivity which is highly dependent on temperature [42] [43] [31] [44] [45]. These two mechanisms occur with oxygen diffusion to grain boundaries and creating more brittle layers which behave more brittle and cause early failures.

High-temperature conditions do not always include oxidation effects, under high temperature additional to oxidation, cavity formations across grain boundaries may occur. To observe that, static loading conditions have to be maintained which is also named creep. In addition to that life-reduction amount is depending on the temperature change since the Oxygen diffusivity is depending on the temperature. This temperature change can be determinative also for the crack propagation behavior. For Inconel718 material above 500 $^{o}$C temperature crack propagation exhibits transition from cycle-dependent transgranular to time-dependent intergranular propagate characteristics [42]. Since the tests are performed below these temperatures for the cyclic fatigue test transgranular crack growth is expected. Yet in some papers, axial fatigue test results have resulted similarly for 350 $^{o}$C and 550$^{o}$C [46].

Behavior change with increasing the temperature can be explained in a couple of fracture mechanisms. With increasing the temperature dislocations will be more mobile and more slip planes becomes active [36] with this activation in un-notched specimen intrusions-extrusion formation will occur faster. Stress accumulations also will be much more faster at the surface, after crack nuclei created oxygen attack to

crack tip effect crack growth as well. Besides that mechanism in both room temperature and high temperatures Inconel 718 material is observed to be softening material [47]. In load-controlled test conditions, this softening behavior of material will cause an increase in plastic strains in each cycle and the hysteresis loops of the specimens will shift to the right-hand side during all the tests until fracture, which is called ratcheting. In these cases, if the applied loads are relatively high and failure eventually will occur however the main governing mechanism of this failure will be excessive deformation rather than cyclic loading [15].

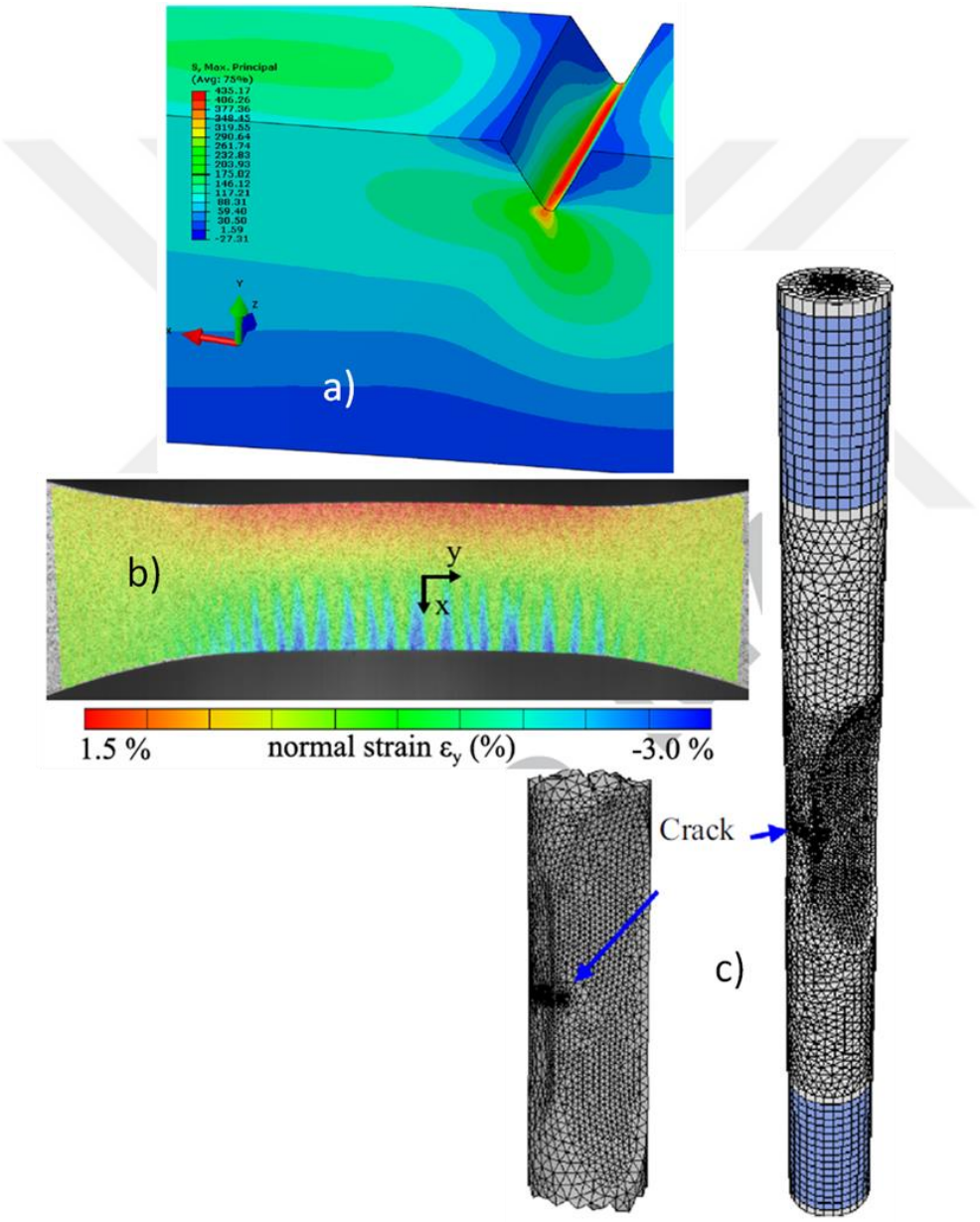


**Figure 4.4 :** Stress distributions of different loadings and specimen geometries; a) Stress distribution notched bending&torsion b)round specimen's pure bending condition c) Edge Notched $K_b$ Bar specimen stress distribution fully under tensile loading [48] [49] [50].

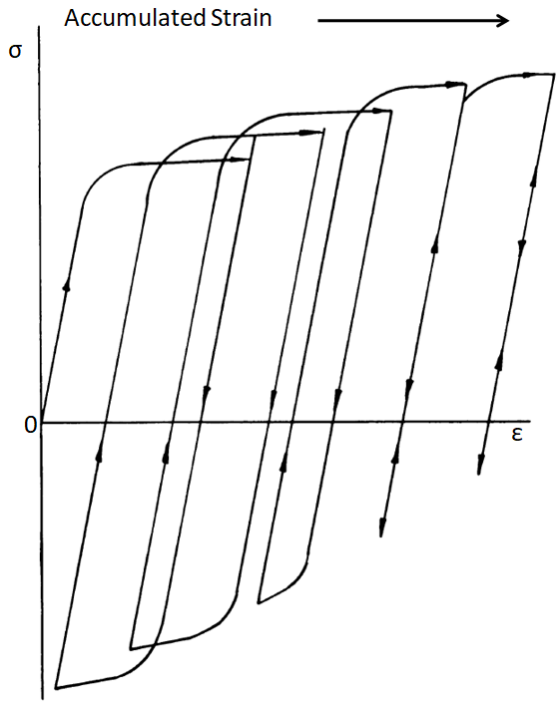


**Figure 4.5 :** Subsequent stress loading corresponding strain accumulations (Ratcheting) [15].

Softening mechanisms of this material is explained by shearing of the gamma double prime precipitates by dislocations in which the sheared precipitate is one of the main strengthening precipitate of the alloy yet is the unstable [51].


**Figure 4.6 :** Schematically expression of Block test [44].

For this intermediate temperature (450$^{o}$C) in which the dislocation volume and mobility is relative high and also the number of active slip bands are increased it is expected to observe life reduction as observed in many literary works which are focused more on crack propagation [52] [53]. In these works, tests are mostly performed under trapezoidal waveform which is schematically described in Figure 4.7**,** and with using notched specimen for focusing on crack propagation than initiation. In the same study, it is shown that an increase in the crack propagation rate is highly dependent on dwell duration and test temperature. An increase in temperature or dwell duration increases the crack propagation rate [31].

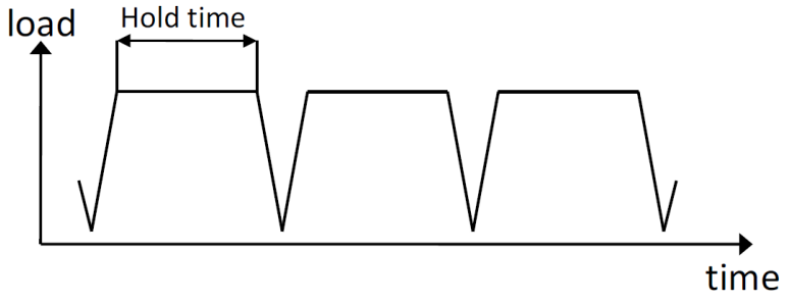


**Figure 4.7 :** Schematically expression of Trapezoidal test [44].

In engineering applications, some parts suffer under tensile dwell loading and some of them suffer compressive dwell loading. For different conditions materials dwell sensitivity can change. For instance in literature, while MARM-002 shows nearly negligible dwell sensitivity at 750$^{o}$C under compressive loadings, Waspalloy shows a drastic reduction in life under both tensile and compressive dwell loadings. This comparison is made by calculating Normalized Cycle Ratio (NCR) which dwells fatigue life divided by the non-dwell result. Like these examples also Rene 80 shows a clear reduction in life when subjected to dwell conditions both in tensile and compression, yet Rene 95 shows relatively nearly equal to 1 values under tensile dwell conditions at 650$^{o}$C. It is important to note that Waspalloy and Rene 95 are cyclically softening materials like Inconel718 alloy. Apart from alloy type, It is observed that an equal amount of applied tensile and compressive dwell application causes relatively low dwell sensitivity [53]. An increase in life under dwell conditions can be explained by crack closure which is also examined widely in literature works. Since the crack propagation is relatively dependent on the stress intensity factor range behind the crack tip, decreasing the effect of this stress intensity factor also will also be expected to reduce crack growth rate. The magnitude of compressive stresses behind the crack tip changes the active stress intensity factor and changes the crack growth [31].

Another work which is also performed in Linköping University shows that the loading application under the Block test waveform shows different crack propagation behavior, which indicates higher crack propagation in early periods of test after a certain time crack propagation rate reaches pure fatigue rates. Which can be related to materials cyclic response. Similar to this work it can be expected that after cyclic response the crack propagation rates may be affected by dwell periods [45].

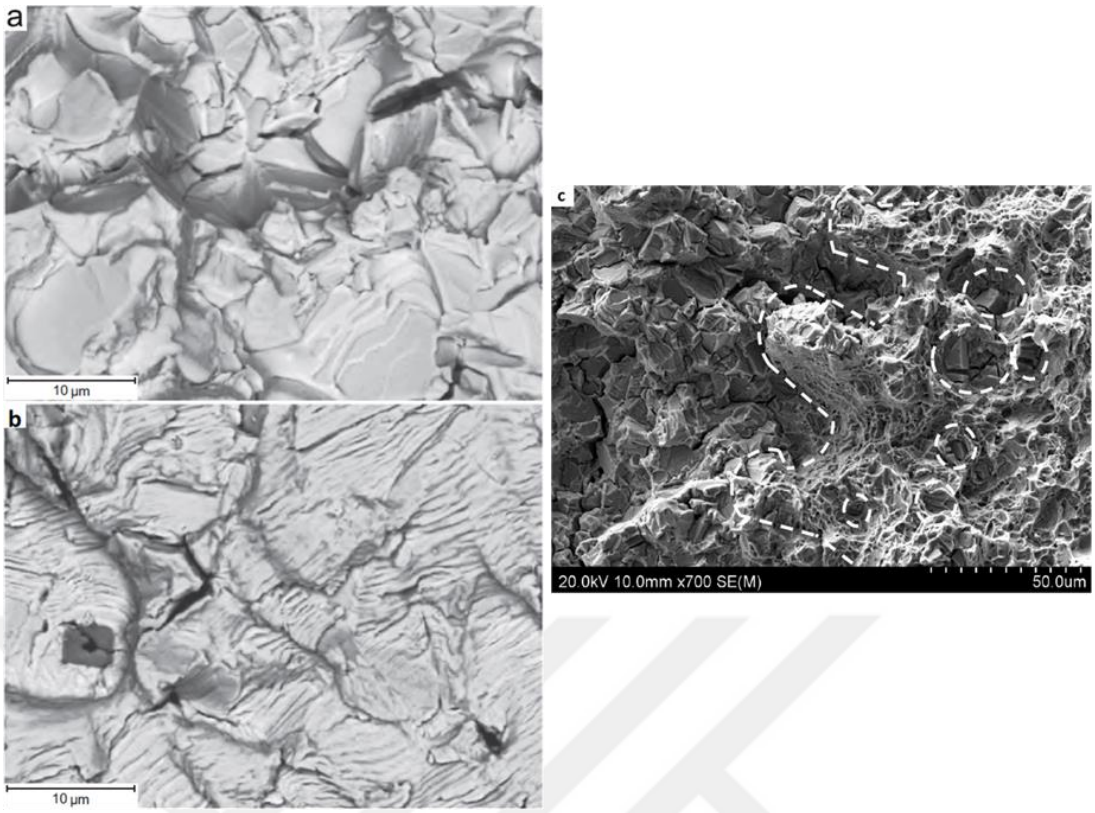


**Figure 4.8 :** SEM imaging of fracture surfaces a) Trapezoidal wave form 2160sec dwell application at 550$^{o}$C , b)Pure axial fatigue at 550$^{o}$C [52] c) Block Test at 550$^{o}$C [44].

In Figure4.8 a and b striations are reduced drastically means that with dwell application fracture mechanism is becomes more time-dependent than cycle-dependent. In the same figure c under block test conditions, it is clear that irregularities at the crack path are seen with mixed fracture surfaces. This mixed fracture surface includes intergranular smooth propagation zones and also transgranular regions with a more ductile appearance [44]. In scientific works which include Inconel718 fatigue and dwell conditions observed irregularities at the crack front. This irregular crack growth shows visible transgranular and intergranular regions through the crack path [52].

## 5. EXPERIMENTAL PROCEDURE

Specimens are manufactured from Inconel718 bar formed materials which subjected to heat treatment as follows; Solution heat treatment between 941-1010ºC then air cooling, heating to temperatures between 718 to 760ºC then 8 hours holding at these temperatures then cooling is applied with rate of 56ºC per hour then 8 hours holding is performed at temperatures between 621 to 649ºC then air cooling is applied. [AMS 5663] After heat treatment machining is performed in accordance with ASTM E606 & E466 and further NADCAP (Code Z) requirements. Specimen initial mechanical properties are given in Table.1. Specimen diameter is aimed to get 5.08 mm and the rest of the dimensions are maintained according to diameter. The Gage length is 12 mm and the total length of the specimen is approximately 100mm. After machining of the specimens, low stress grinding and polishing in the longitudinal direction is performed in TUSAS Engine Industries.

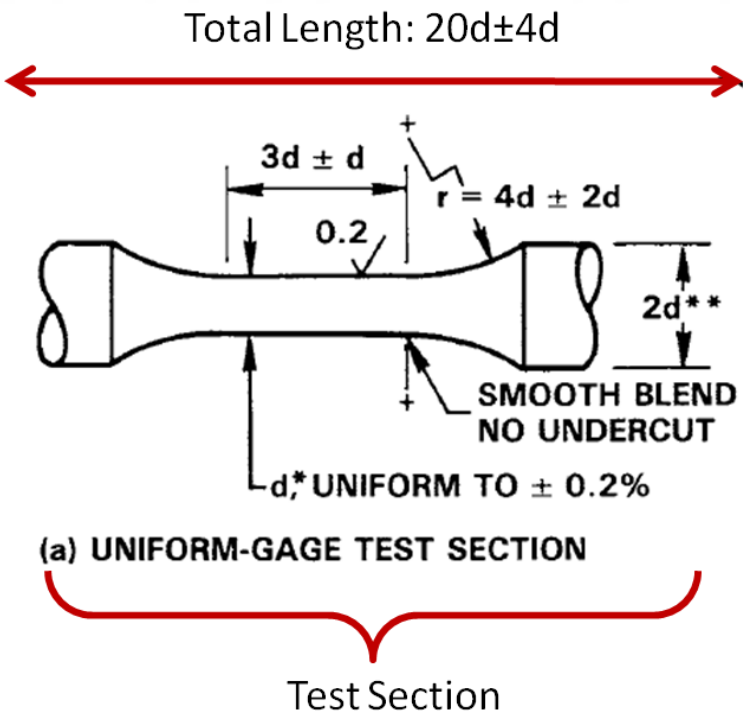


**Figure 5.1 :** Schematically descriptions of Fatigue specimen.

After specimen manufacturing load controlled fatigue tests are performed with W+B Walter Bai Ag Rotating bending test machine. Loading is applied with dead weights and heating is performed one zone electrical resistance furnace. Before the test start additional to furnace control K type thermocouple, another K type thermocouple is used to measure test start temperature on the specimen gage.

Test Rig is basically includes items down below;

1. Oil circulation, bypass hose connections
2. Fixtures, for specimen assembly
3. Testing zone
4. Electrical resistance heaters
5. Displacement sensor, to detect specimen fracture
6. Loading arms

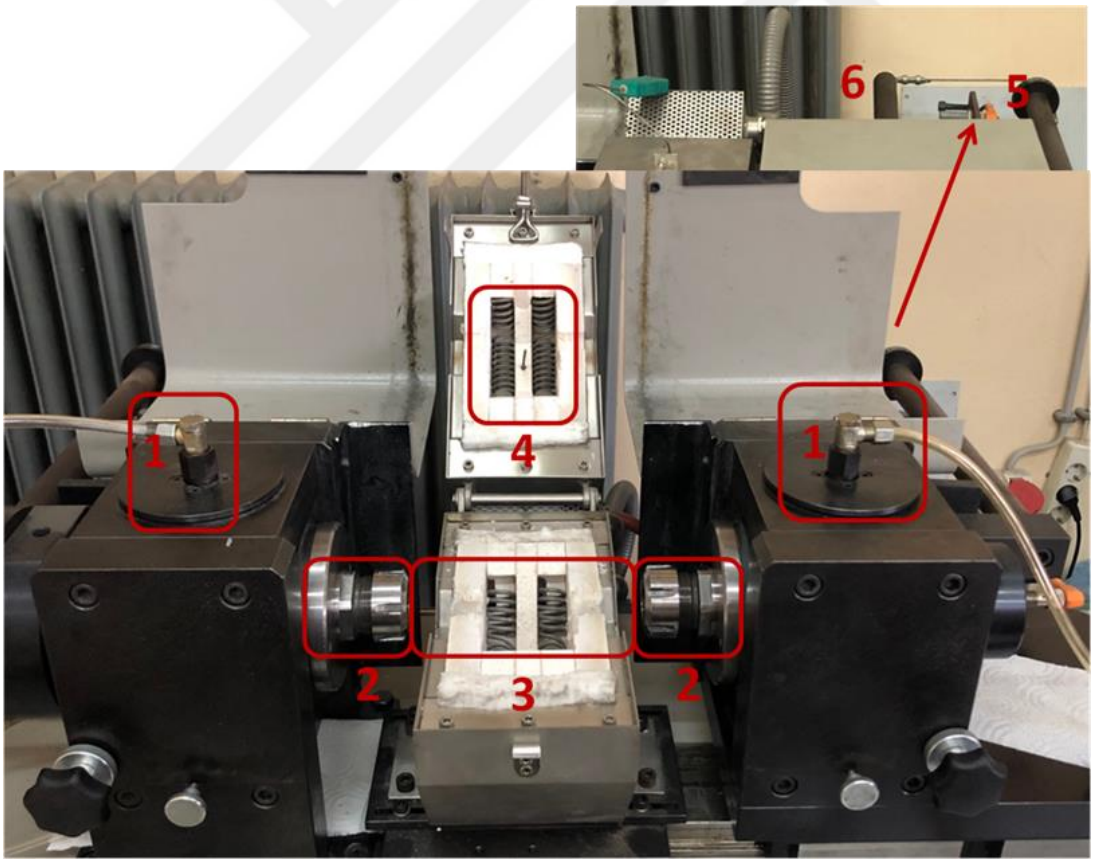


**Figure 5.2 :** Test Setup and equipment overall.

**Table 5.1 :** Initial Mechanical properties of Inconel718.

| Temperature | Room Temperature | 450°C |
|---|---|---|
| UTS (Mpa) | 1400 | 1240 |
| E Modulus (Gpa) | 204 | 180 |
| Elongation (%) | 20.9 | 22.6 |
| Yield Strenght (Mpa) | 1150 | 1030 |

In Figure 5.3 additional thermocouple measurement and measurement, the point is shown. The specimen is heated using 2 temperature steps, these two steps are used to reach the target temperature within one hour. After reaching the first temperature 15 minutes of soaking is applied. After reaching the final target temperature 30 minutes of soaking time was applied to make sure the temperature distributions. It is observed that there is a deviation between furnace temperature and used additional thermocouple values. To maintain target temperature more relevant temperature profile work is applied. After examining the furnace for nearly 20 hours it is concluded that for 450°C specimen temperature approximately 530°C target temperature should be given to furnace.

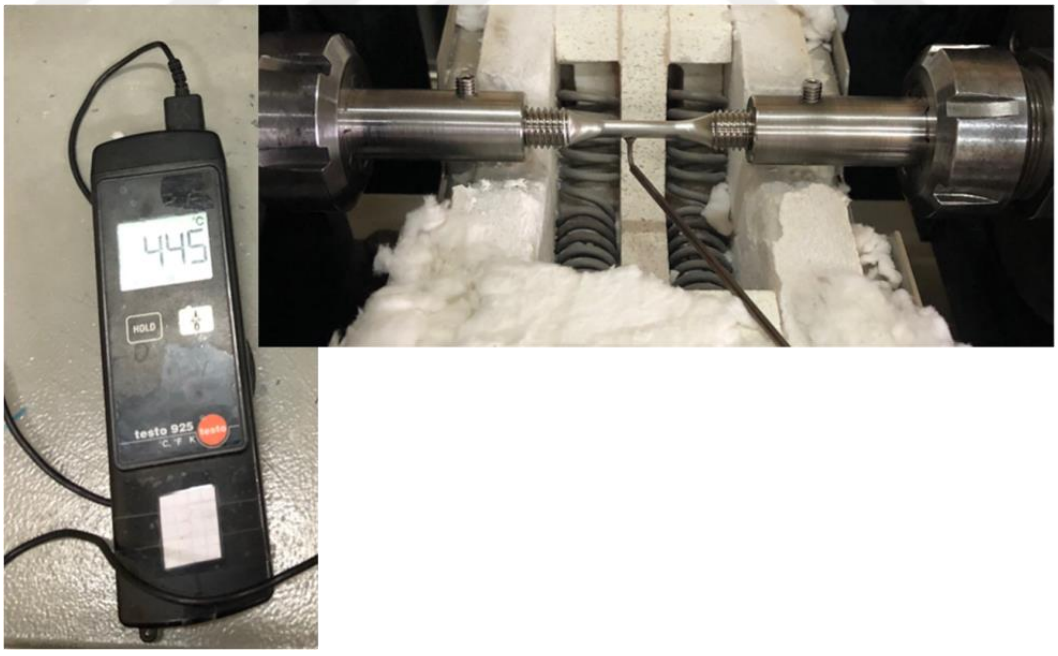


**Figure 5.3 :** Additional thermocouple application.

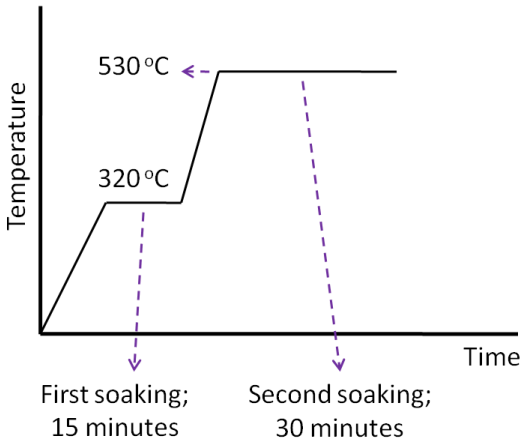


**Figure 5.4 :** Heating profile, first and second target temperatures to reach specimen temperature 450 °C.

After performing standard fully cyclic fatigue testing dwell fatigue testing is performed. To simulate this, the driving electrical motor stopped during certain periods. After fatigue testing, subsequent hardness measurements, profilometer measurements, nanoindentation, microstructural examinations, and SEM visualizations are performed. Hardness measurements are performed to observe any mechanical strength change.

Specimens are prepared after hot molding, grinding is performed from 120 grid sandpapers to 1200 grid sandpapers, after grinding 6 and a 1-micrometer diamond solution is used. To observe fatigue damage accumulation surface conditions are measured with Dektak 6M profilometer. Specimens initial surface roughness values are 0,2Ra profilometer results are given in further chapters.

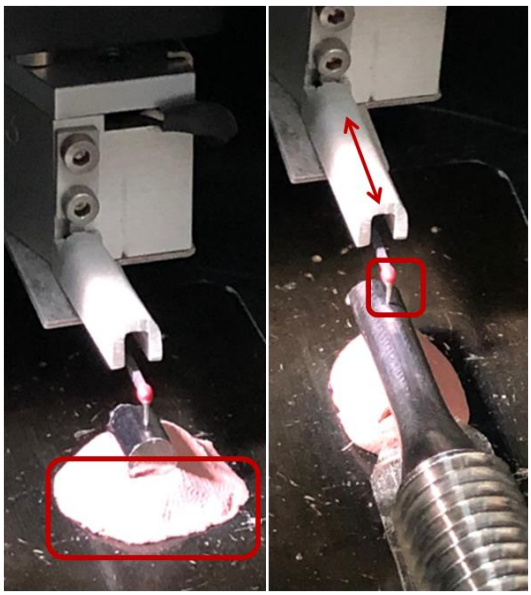

**Figure 5.5 :** Profilometer setup; mold, indenter and indenter movement is marked.

Hardness measurements are performed with 0.98 Newton results are given in further chapters. Hardness measurements are performed in certain regions of molded specimens, measurements are performed from perpendicular direction to loading axis. I-II-III regions are represents subsequently; closer to fracture surface, middle regions, far from testing center.

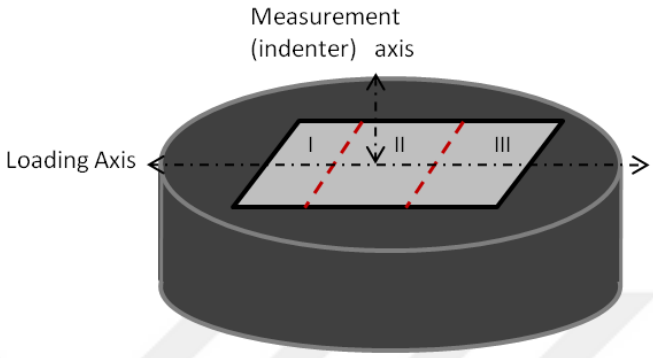


**Figure 5.6 :** Schematically description of hardness testing specimens and loading axis respectively.

After these measurements Nano indentation measurements are performed in order to observe any change in toughness. Tests are performed with using maximum load level of 0.5 mN. Test are performed with 10 repetitions, results are shared in further chapters.

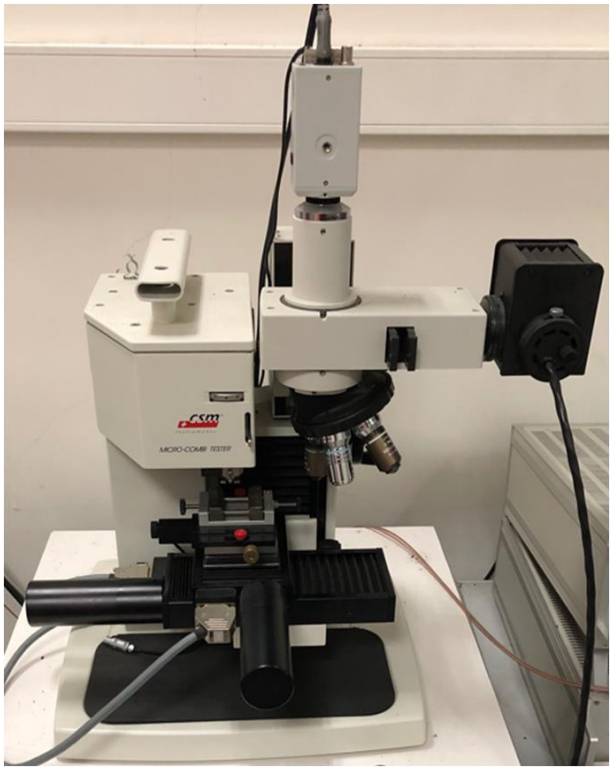

**Figure 5.7 :** CSM Micro-Combi tester nano indendation testing machine.

Molded specimens are then re polished and etched with using acidic solution which includes; 50ml methanol, 5 ml $H_2O_2$, 50ml HCl. After etching grain size measurement is performed according to ASTM E112, comparison procedure is used with 100X magnified visuals three different regions as described in hardness measurement.

## 6. RESULST & DISCUSSION

Load-controlled rotating bending fatigue tests are performed from room temperature condition to high-temperature dwell tests, to specimens which are prepared according to ASTM E466 standard. In rotating bending fatigue conditions specimen's surface is subjected to tensile and compressive stresses at the same time. Test results are given in Table6.1 At room temperature endurance limit can be accepted as 500Mpa since the test specimen has not suffered any fracture, also the ratio between stress amplitude and ultimate tensile stress of the material is approximate; 0.36 and this result is compatible with literary works.[54] *Used "*"refers to the tests that are not fractured,*

**Table 6.1 :** Performed fatigue and dwell fatigue test results.

| Test Number | Test Temperature | Test Condition | Stress Amplitude (Mpa) | Stress Amplitude / Yield Stress | Frequency (Hz) | Normalised Cycles |
|---|---|---|---|---|---|---|
| 1 | RT | Non-Dwell | 1094 | 0.95 | 30 | 0.79 |
| 2 | RT | Non-Dwell | 998 | 0.87 | 30 | 0.87 |
| 3 | RT | Non-Dwell | 771 | 0.67 | 30 | 0.99 |
| 4 | RT | Non-Dwell | 677 | 0.59 | 30 | 1.07 |
| 5 | RT | Non-Dwell | 600 | 0.52 | 30 | 1.13 |
| 6 | RT | Non-Dwell | 502 | 0.44 | 30 | 1.36* |
| 7 | RT | Non-Dwell | 559 | 0.49 | 30 | 1.32 |
| 8 | RT | Non-Dwell | 771 | 0.67 | 30 | 1.00 |
| 9 | RT | Non-Dwell | 600 | 0.52 | 30 | 1.16 |
| 10 | RT | Non-Dwell | 677 | 0.59 | 30 | 1.07 |
| 11 | RT | Non-Dwell | 560 | 0.49 | 30 | 1.26 |
| 12 | RT | Dwell Fatigue | 560 | 0.49 | 60 | 1.21 |
| 13 | RT | Dwell Fatigue | 560 | 0.49 | 30 | 1.15 |
| 14 | RT | Dwell Fatigue | 560 | 0.49 | 30 | 1.03 |
| 15 | RT | Non-Dwell | 560 | 0.49 | 30 | 1.19 |
| 16 | 450°C | Non-Dwell | 636 | 0.62 | 19 | 0.90 |
| 17 | 450°C | Non-Dwell | 600 | 0.58 | 17 | 1.08 |
| 18 | 450°C | Non-Dwell | 600 | 0.58 | 17 | 0.75 |
| 19 | 450°C | Non-Dwell | 771 | 0.75 | 17 | 0.95 |
| 20 | 450°C | Non-Dwell | 771 | 0.75 | 17 | 0.91 |
| 21 | 450°C | Non-Dwell | 502 | 0.49 | 17 | 1.30 |
| 22 | 450°C | Dwell Fatigue | 771 | 0.75 | 17 | 0.93 |
| 23 | 450°C | Dwell Fatigue | 771 | 0.75 | 17 | 0.96 |
| 24 | 450°C | Non-Dwell | 600 | 0.58 | 17 | 1.18 |
| 25 | 450°C | Non-Dwell | 771 | 0.75 | 17 | 0.91 |
| 26 | 450°C | Dwell Fatigue | 600 | 0.58 | 17 | 1.11 |
| 27 | 450°C | Dwell Fatigue | 600 | 0.58 | 17 | 1.14 |
| 28 | 450°C | Non-Dwell | 560 | 0.54 | 17 | 1.24 |
| 29 | 450°C | Dwell Fatigue | 502 | 0.49 | 17 | 1.33 |
| 30 | 450°C | Dwell Fatigue | 560 | 0.54 | 17 | 1.35* |
| 31 | 450°C | Non-Dwell | 560 | 0.54 | 17 | 1.35* |
| 32 | 450°C | Non-Dwell | 831 | 0.81 | 17 | 0.89 |
| 33 | 450°C | Dwell Fatigue | 502 | 0.49 | 17 | 1.35* |

After gathering results, the best fit calculation is performed to find the data which represent observed populations. Best-fits are calculated with using subsequently; power-law relation, exponential relation, Manson's Equal Slopes, and Linear fitting according to ASTM E739. Different best fit calculations are compared in terms of coefficient of determination ($R^2$) and distances from raw data using the summation of squared residuals.

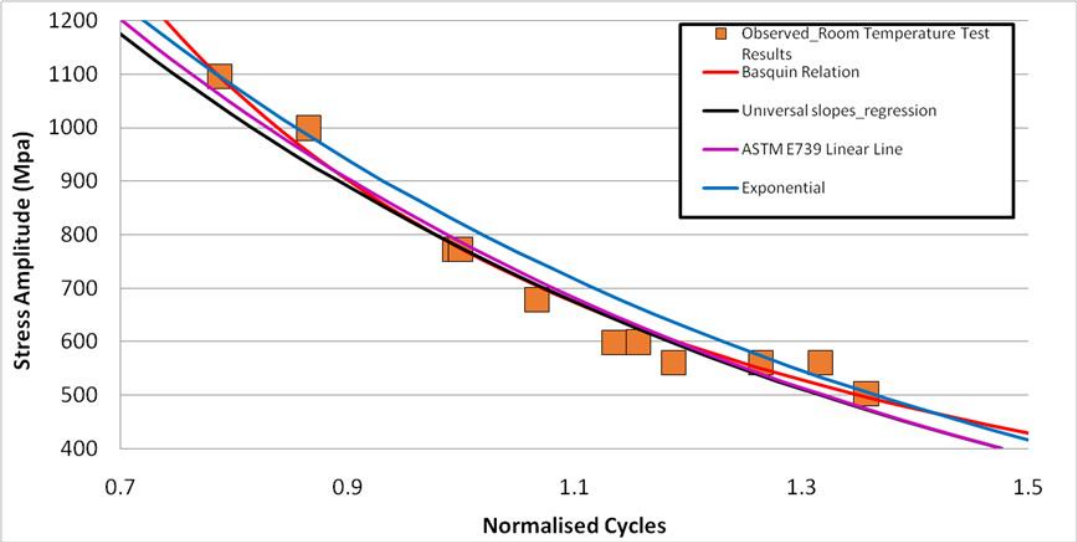


**Figure 6.1 :** Comparison of different best fits on room temperature test results.

As seen in Figure 6.1 according to raw data distribution, different model equations can work on this certain data set, in this case, quantitative comparisons must be made. In this work summation of squared residuals (SSR) and coefficient of determination ($R^2$) were used for this comparison. Fallowing equations 6.1 and 6.2 are used.

$$SSR = \sum_{i=0}^{n} \left(\log N_p - \log N_o\right)^2 \tag{6.1}$$

$$R^2 = 1 - SSR \Big/ \sum_{i=0}^{n} (y_i - \bar{y})^2 \tag{6.2}$$

$$\bar{y} = \frac{1}{n} \times \sum_{i=0}^{n} y_i \tag{6.3}$$

**Table 6.2 :** Calculated SSR & $R^2$ values.

| Room Temperature Data Process Results | | | | |
|---|---|---|---|---|
| | Power Law/Basquen | Universal slopes_regression | ASTM_E739 | Exponential relation |
| SSR | 1.066 | 0.406 | 0.518 | 0.502 |
| $R^2$ | 0.915 | 0.968 | 0.959 | 0.96 |

According to Table 6.2 in this case, by comparing the SSR values "Power Law" method was observed to be appropriate however with calculating the probability curves the ASTM E739 method can be selected. Also comparing the $R^2$ value it can be said that all model equations sufficiently represent test results since all of them explain the observed data above 90 percent. In terms of analyzing the data, there are some different approaches especially for determining the outliers such as; box plots examinations, t distribution test, F test, etc. In this work, box plot examination is used to determine if the certain data is an outlier or not. In Figure 6.2 it can be obtained that for ASTM Linear, Power-law, Manson's Equal Slope's there is no certain data that can be considered as an outlier from the data curve. Only in the Exponential model equation, 1 observation is calculated distant from mean data according to box-plot, however, comparing the studentized T values shows there are two outlier data in the ASTM E739 method but with comparing the 99% probability plots ASTM methodology can be accepted as seen in Figure 6.3**.**

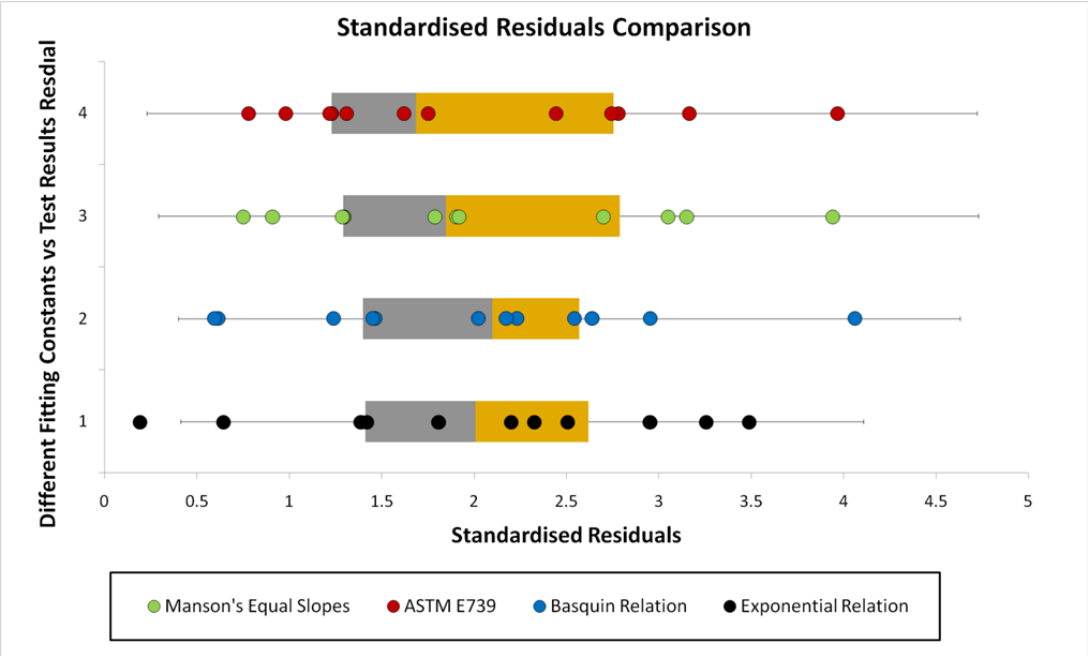


**Figure 6.2 :** Box Plots of different model equations on Room temperature fatigue test results.

Calculating the best fit from different model equations will give slightly different solutions, however, there is no certain answer for that, different model equations can work in the same data set. Nevertheless, some items have to be kept in mind. While defining the materials certain mechanical property extrapolations to regions where no observation exists are considered as an unsafe approach.

**Table 6.3 :** Studendized T Outlier comparison according to Chapter 3 with significance of 0.05.

| Critical TC | Absolute Ti | Applied Stress (Mpa) | Normalized Cycles to failure |
|---|---|---|---|
| 0.977 | 0.457 | 1094 | 0.79 |
| | 0.730 | 998 | 0.87 |
| | 0.385 | 771 | 0.99 |
| | 0.774 | 677 | 1.07 |
| | 1.215 | 600 | 1.13 |
| | 0.858 | 502 | 1.36 |
| | 1.607 | 560 | 1.32 |
| | 0.517 | 560 | 1.26 |
| | 0.269 | 771 | 1.00 |
| | 0.740 | 600 | 1.16 |
| | 0.785 | 677 | 1.07 |
| | 0.909 | 560 | 1.19 |

These approaches are applied to all test results in this work. When examining the high-temperature results it can be seen that the repeatability of high-temperature specimens is low. Increasing the temperature in the test environment creates more challenging conditions and in which increases the scatter in tests. After applying the same procedures on high-temperature observations, high temperature and room temperature data are compared in terms of best fit and raw data in Figure 6.5. In Figure 6.4 high-temperature test results and calculated curves can be seen. Increasing distance between probability curves is evidence to increasing in the scatter of the data.

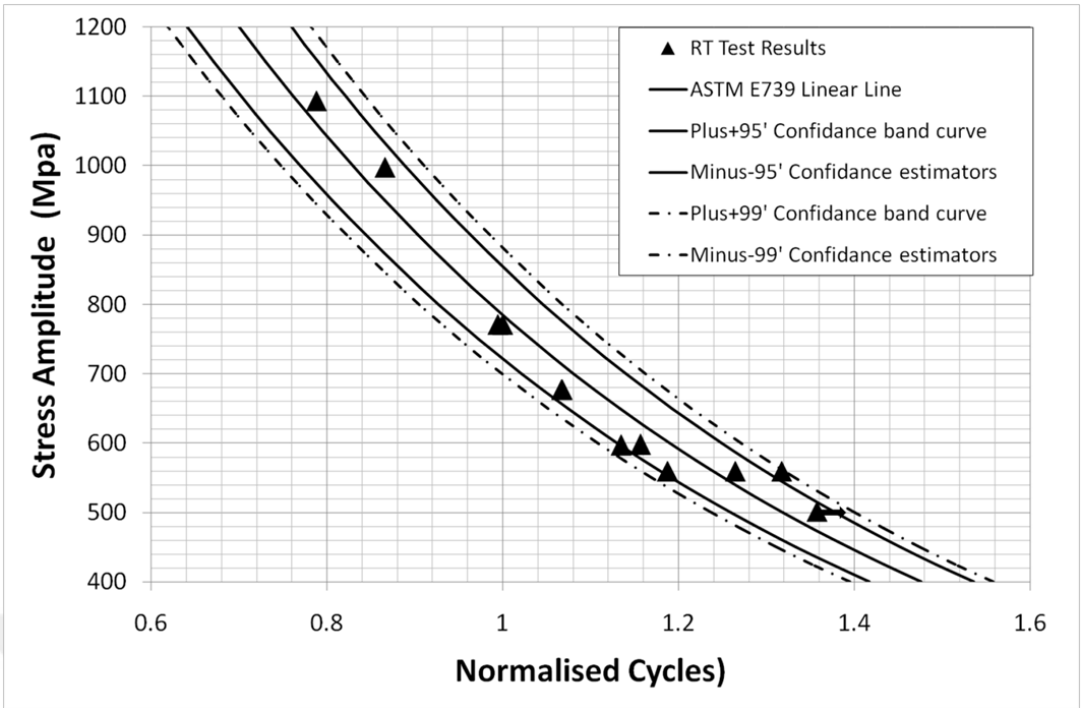


**Figure 6.3 :** Room Temperature data set, best fit, and 0.95-0.99 probability curves calculated according to ASTM E739.

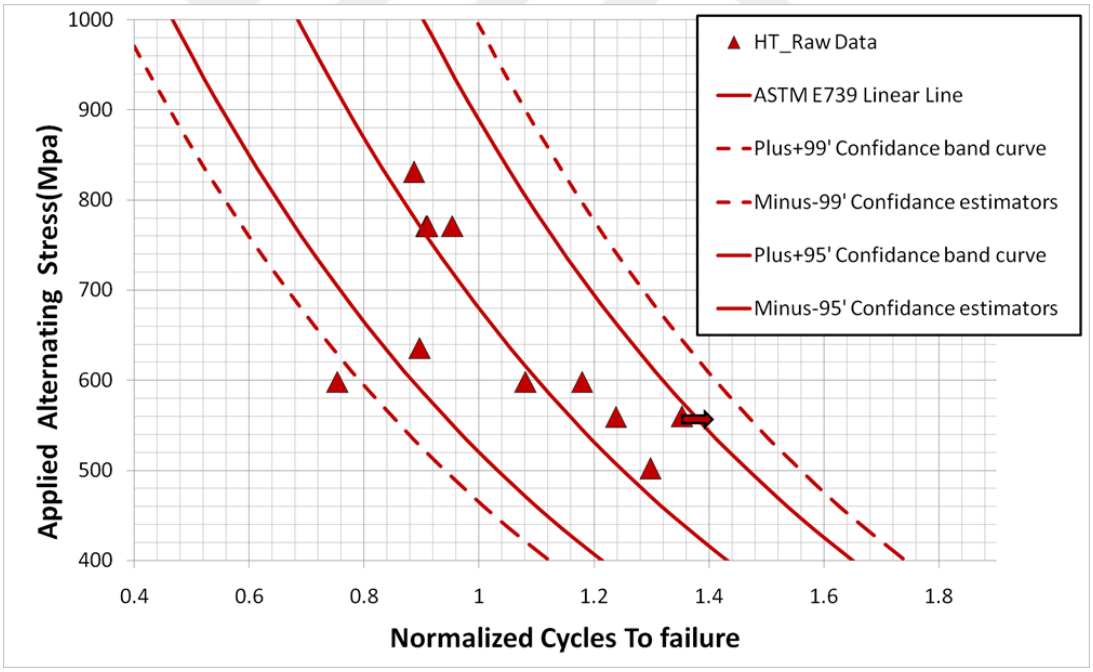


**Figure 6.4 :** High Temperature (450$^{o}$C) data set, best fit, and 0.95-0.99 probability curves calculated according to ASTM E739.

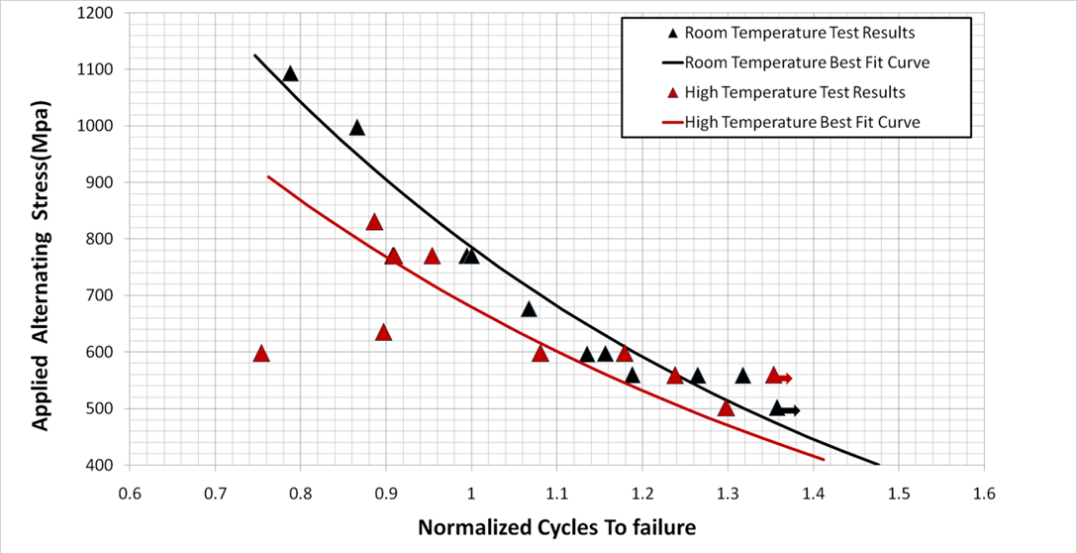


**Figure 6.5 :** High Temperature (450°C) data set, best fit and Room Temperature data set, best fit comparison.

In Figure 6.5 calculated best fit curves extended to understand the difference in different data trends more clearly. Figure 6.5 is evidence on environmental factors are highly effective on materials cyclic behavior. According to the best-fit curves, it seems there is a constant percentage difference between room temperature and the 450°C curve. This percentage can be approximated to a %12 reduction with increasing the temperature up to 450°C. It has to be noted that with decreasing the stress level the differences between life results seem to be decreasing however data points which are visualized with arrows are the "Run Out" tests which means the specimens did not suffer any fracture, specimens removed from the test the rig after 6-7*106 cycles. Knowing that in terms of endurance limit the difference between room temperature and high temperature would also seem to be intersecting.

After observing the fully cycle-dependent failure behavior of the material, dwell periods are added to the test matrix. Dwell fatigue tests are planned to simulate the engine's operating stress levels by holding the specimen at max load for the duration of dwell. Instead of applying the static hold in each cycle, to observe the cyclic and static response of the material separately "Block" test method is used which is described in Figure 6.6. Dwell durations are chosen with a proportion of the estimated test duration. Applied load dwells and test durations are given in Table 6.4. For different test durations and different loading levels cyclic and dwell period length is changed in unit minutes. The aim of increasing the dwell periods is to increase the time-dependent mechanisms. In this period specimen surface is subjected to both

tensile and compressive stresses which also has a different effect on the material's cyclic behavior.

**Table 6.4 :** Performed Dwell Test's Parameter Comparisons.

| Test Number | Temperature (°C) | Cyclic Loading Durations (Minutes) | Dwell duration (Minutes) | Total Dwell Duration (Minutes) | Total Cyclic Test Duration (Minutes) | Test Frequency | Dwell / Cyclic Ratio |
|---|---|---|---|---|---|---|---|
| 12 | Room Temp. | 30 | 60 | 420 | 360.6 | 60 Hz | 1.16 |
| 13 | Room Temp. | 30 | 60 | 420 | 348.5 | 30 Hz | 1.21 |
| 14 | Room Temp. | 30 | 60 | 240 | 140 | 30 Hz | 1.71[a] |
| 20 | 450 | 10 | 10 | 60 | 68.4 | 17 Hz | 0.88 |
| 21 | 450 | 10 | 10 | 50 | 47.6 | 17 Hz | 1.05 |
| 24 | 450 | 30 | 45 | 315 | 382.1 | 17 Hz | 0.82 |
| 25 | 450 | 30 | 45 | 315 | 533.6 | 17 Hz | 0.59 [a] |
| 27 | 450 | 30 | 60 | 420 | 6517.4 | 17 Hz | 0.06[b] |
| 28 | 450 | 30 | 60 | 420 | 5025.4 | 17 Hz | 0.08[b] |
| 33 | 450 | 30 | 60 | 420 | 6343.1 | 17 Hz | 0.07[b] |

*Used "a"refers to the early failure and "b" refers to "Run Out" tests.*


**Figure 6.6 :** Schematically expression of Block test [44].

Table 6.4 shows applied dwell durations in comparison with cyclic periods and total test durations. It can be seen from the table that some of the tests has early failures and in some tests, cyclic life increased dramatically. For most of the tests, the ratio between total dwell duration and total cyclic duration aimed to be maintained between "0,8-1,2" in average "1". For the tests that have 420 minutes of dwell time, the ratio is relatively close to "0" because after dwell application these tests are not suffered any fracture these tests can be considered as "Run Out Tests".

In Figure 6.7 for high-stress levels, it can be assumed that failure has dominantly occurred in cycle-dependent mechanism since the final life of the test has no significant change. With decreasing the stress levels difference between base tests and dwell fatigue tests are more visible. For this intermediate temperature (450°C) in which the dislocation volume and mobility are relatively high and also the number of active

slip bands are increased it is expected to observe life reduction as observed in many literary works which are focused more on crack propagation [31] [53].

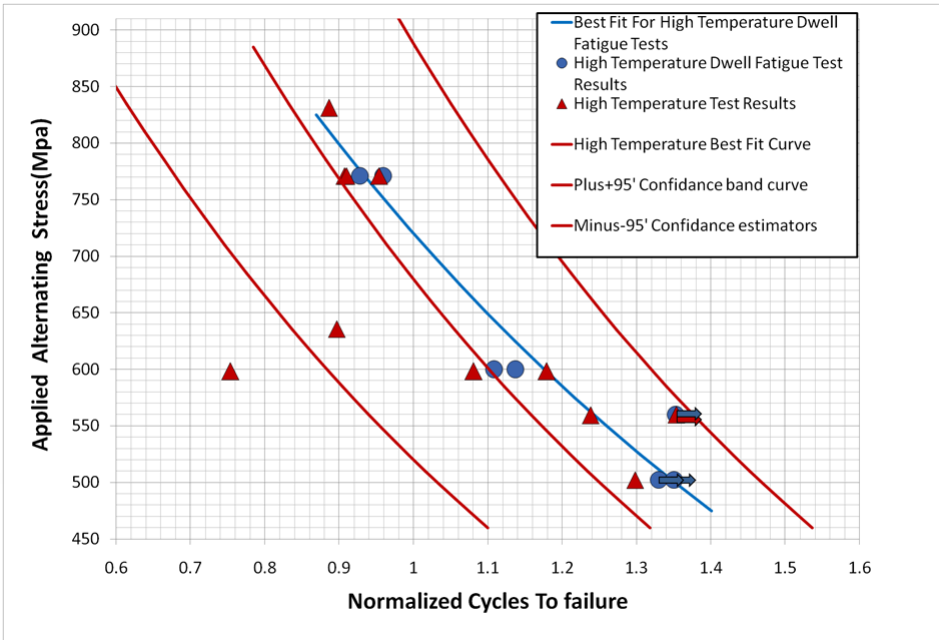


**Figure 6.7 :** High Temperature (450°C) Dwell and Non-Dwell Fatigue Test Results with Best Fits.

Unlike in 450°C at room temperature dwell fatigue tests showed relatively lower life results which can be seen in Figure 6.8. These results are near the ±95% probability lines but it is clear that the mean of the room temperature dwell fatigue results are lower than non-dwell fatigue tests.

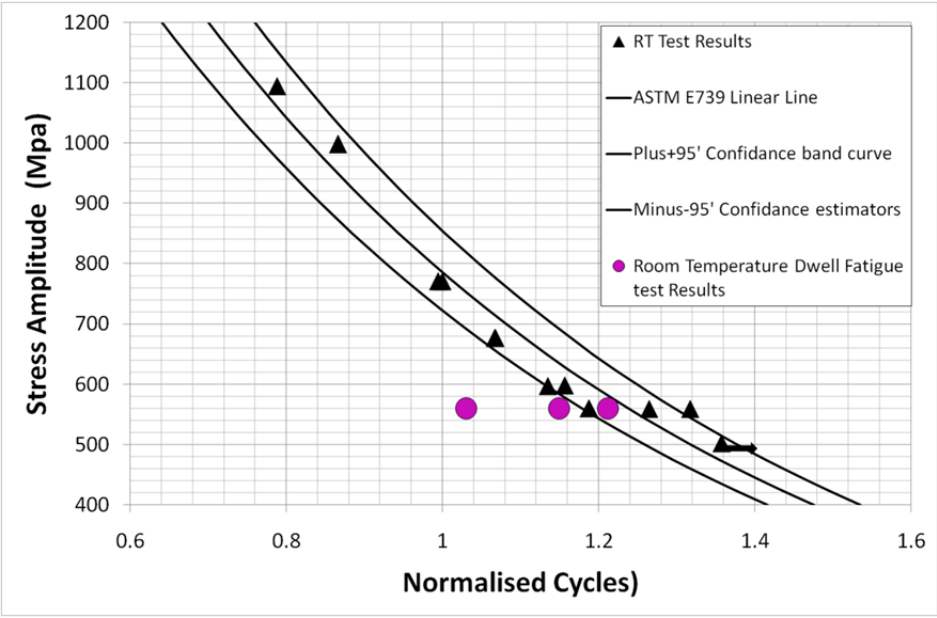


**Figure 6.8 :** Room Temperature fatigue and dwell fatigue test comparison with best fits.

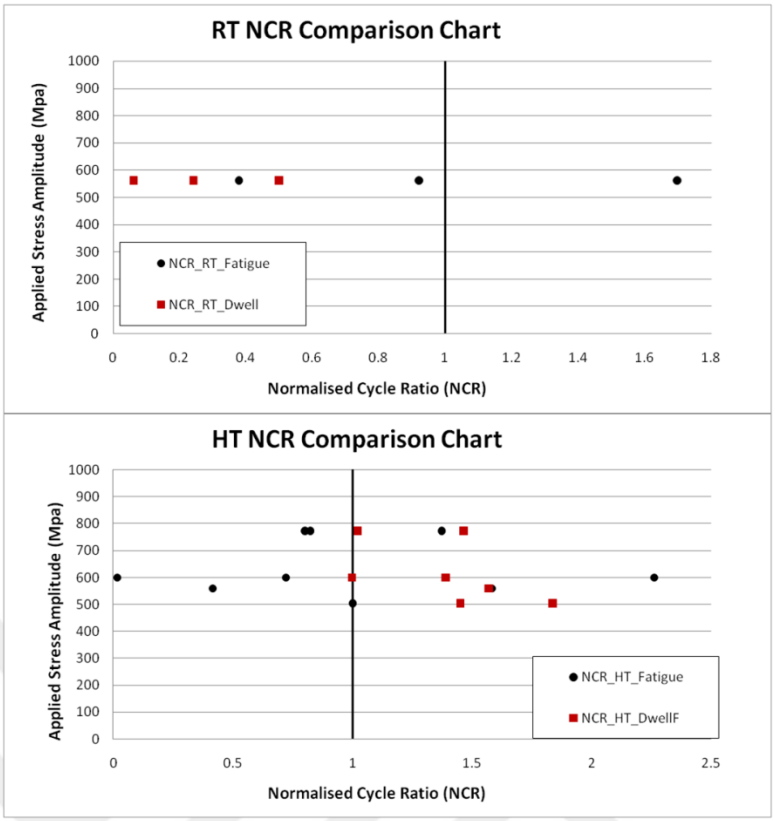


**Figure 6.9 :** Room temperature and High Cycle (450$^{o}$C) dwell sensitivity graphs with calculated NCR comparisons.

In engineering applications, some parts suffer under tensile dwell loading and some of them suffer compressive dwell loading [53]. For different conditions materials dwell sensitivity can change. This comparison is made by calculating Normalized Cycle Ratio (NCR) which is dwell fatigue life divided by the non-dwell result. In Figure 6.9 at room temperature life, the reduction is clear. Compressive and tensile balanced dwell loadings seem to be more effective at room temperature conditions. High temperature calculated NCR values are evidence for stress magnitude dependency of dwell sensitivity for Inconel718. Even the NCR values show dwell sensitivity clearly, when examining the life results and room temperature best fit & percentile curves, one of the dwell results seems to be equivalent with the best fit.

Material's cyclic behavior change can be seen for different test conditions. Change in life results can be caused by different factors. Since the fatigue behavior is also dependent on material overall strength, to understand these results further hardness measurements have been performed. Hardness measurements are performed in three different measurement zones of fractured specimens, named; I, II, III. These regions represent the distances that are stated in Table 6.5.

**Table 6.5 :** Measurement Zone distance from Failure Surface.

| Measurement Zone | Distance Ranges From Failure Surface (mm) |
|---|---|
| I | 0.15 - 0.23 |
| II | 1.0 - 3.0 |
| III | 2.0 - 4.0 |

**Table 6.6 :** Performed Hardness test results and specimen conditions.

| Test Number | Measurement Zone | Hardness (HV0.1) | Test Condition |
|---|---|---|---|
| 7 | I | 482 | |
| 7 | II | 489 | 560 Mpa - Room Temp. - 1.32Nf |
| 7 | III | 509 | |
| 23 | I | 478 | |
| 23 | II | 482 | 771 Mpa - 450 °C - 0.91Nf |
| 23 | III | 514 | |
| 22 | I | 473 | |
| 22 | II | 477 | 600 Mpa - 450 °C - 1.18Nf |
| 22 | III | 522 | |
| 20 | I | 436 | |
| 20 | II | 452 | 771 Mpa - 60 min Dwell - 450 °C - 0.96Nf |
| 20 | III | 495 | |
| 21 | I | 474 | |
| 21 | II | 462 | 771 Mpa - 50 min Dwell - 450 °C - 0.93Nf |
| 21 | III | 480 | |
| 24 | I | 468 | |
| 24 | II | 486 | 600Mpa - 315 min Dwell - 450 °C - 1.11Nf |
| 24 | III | 491 | |

*I: Closest measurement to fracture surface, II: Middle measurement location, III: Distant measurement point.*

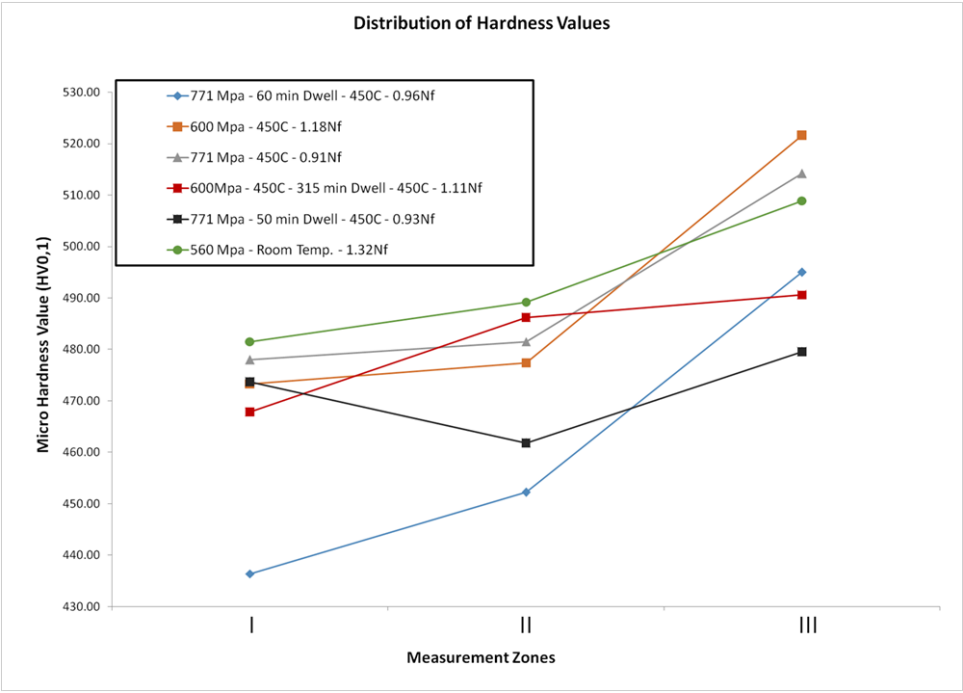


**Figure 6.10 :** Hardness measurements form different distances from the fracture surface.

From Table 6.6 and Figure 6.10 it can be seen that specimens show softening since the material's initial hardness values are approximately 500-520 Vickers. This softening phenomenon can be seen in all test types. With increasing the temperature softening trend also increases its slope, different stress levels also showed different amounts of decrease in hardness value which means softening is a stress-dependent phenomenon. It is important to note that softening is observed at room temperature too which means this phenomenon is not thermally dominated. The specimen which is subjected to dwell also showed lower hardness values than its counterpart without dwell. Change in hardness provides illuminating perspective to understand the cyclic life change however these results raised new questions on material toughness and overall plastic capability. Measured surface roughness values after fatigue testing are observed to be not repeatable enough to gain certain inferences. The results are deviating from 0,05 to 4 Ra.

Recovery and recrystallization are expected in the deformations applied at high temperatures. Although these phenomena depend on temperature and applied load levels, changes in toughness are expected as they change the distribution of dislocations in the material. In this study, indentation and grain size measurements were carried out to understand whether there are similar mechanisms. Indentation tests are compared in terms of load/distance curves and plastic work ratio(PWR). PWR is a ratio between total area under load-displacement curve and unloading curve. PWR is a value that describes material’s plastic deformation ability.

**Table 6.7 :** Plastic Work Ratios (PWR) of Tested Specimens.

| | Specimen Condition | | | |
|---|---|---|---|---|
| PWR | Applied Stress (Mpa) | Test Temperature | Dwell Duration (min) | Normalized Cycles To Failure |
| 0.835 | 502 | 450 ºC | N/A | 1.30 |
| 0.834 | 502 | 450 ºC | 420 | No failure |

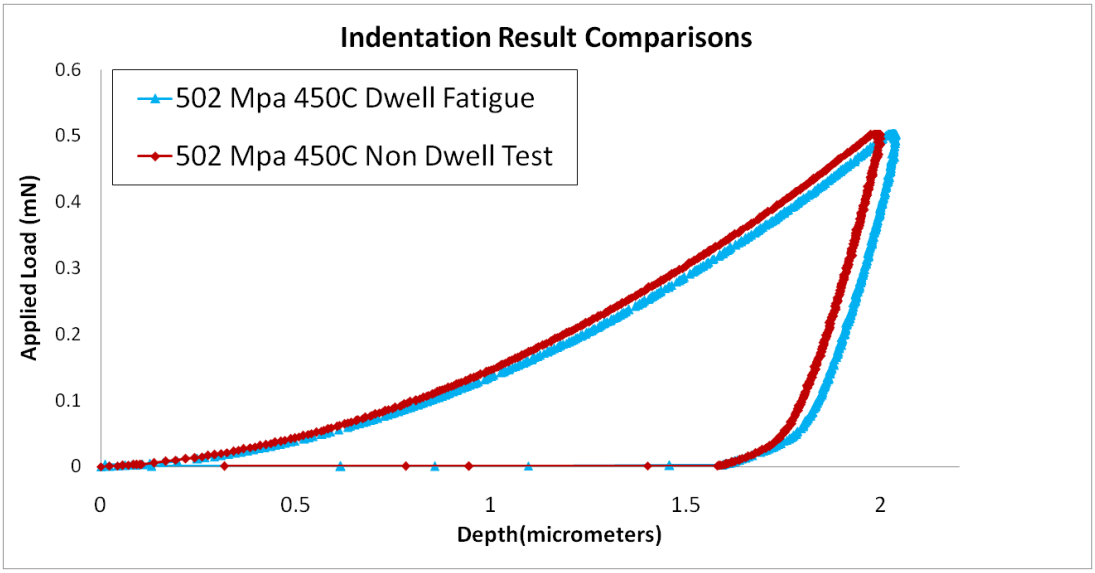


**Figure 6.11 :** Nanoindentation results of high temperature tests.

**Table 6.8 :** ASTM Grain Size number comparison of tested specimens.

| Test Number | Temperature (°C) | Max applied Stress (Mpa) | Dwell Duration (minutes) | ASTM Grain size Number | Uncertainity | Measurement Method |
|---|---|---|---|---|---|---|
| 6 | Room Temp. | 502 | N/A | 9 | ±1 | Comparison (100X graded) |
| 7 | | 560 | N/A | 9.5 | | |
| 12 | | 560 | 420 | 9 | | |
| 13 | | 560 | 420 | 10 | | |
| 27 | | 502 | 420 | 10 | | |
| 19 | 450 | 502 | N/A | 9 | | |
| 28 | | 560 | 420 | 10.5 | | |
| 20 | | 771 | 60 | 9.5 | | |
| 25 | | 598 | 315 | 9.5 | | |

From Figure 6.11 it can be said that even with the increased life results materials toughness is not changed with dwell application. From Table 6.7 interestingly plastic deformation capacities of two different specimens have not changed after 420 minutes of tensile and compressive stress holds. Also, Table 6.8 shows no change in ASTM grain size numbers for specimens used under different test conditions.

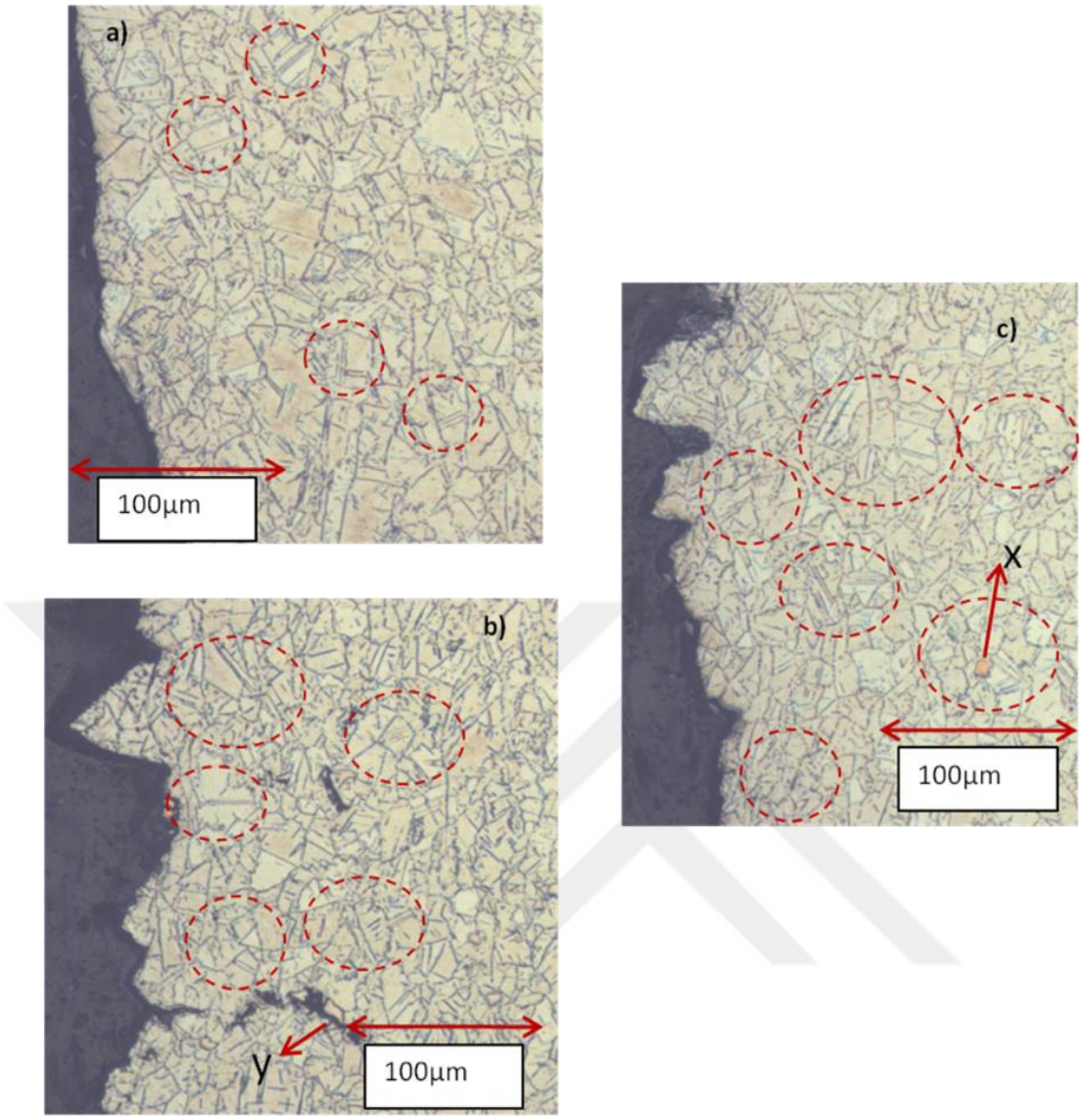


**Figure 6.12 :** Microstructural image of a) Room temperature, 560MPa, 1.32 normalized cycles to failure, b)450$^{o}$C, 771MPa, 0.91 normalzed cycles to failure, c) Dwell fatigue(50mins), 450$^{o}$C, 771MPa, 0.93 normalized cycle to failure, twinning formations expressed in red circles, X stands for Ti rich carbonitride, Y stands for Nb rich carbonitride.

The cause of the material's cyclic life change can also be investigated by examining microstructural monitoring and SEM monitoring. The microstructure of Inconel718 specimens under different test conditions can be seen in Figure 6.12. In this figure with the change of the test condition, the surface topography is also changed. Twinnings are produced after thermomechanical processes during the manufacturing of the material but also it is known that they can be also produced by dislocation movement which causes a decrease in overall strength [36]. Different amounts of twinnings are observed in different test conditions. It is expected that the dislocation mobility and the amount of active slip band increase at high temperatures which creates a favorable

condition for dislocation to shear the existing precipitates. This phenomenon is normally observed during thermomechanical processes at high temperatures and is observed by twinning [36]. Although the softening occurs, it is hard to assume some relation different twinning amounts to softening. In addition to that in the non-dwell test, sub-surface crack is observed near Nb rich carbonitrides meaning the material has a relatively brittle zone where the Nb-Ti rich carbonitrides are formed [55].

In Figure 6.13 it can be observed that fracture topography has no distinctive change along the fracture surface. From that observation, it can be said that fatigue tests without dwell application have a transgranular crack growth mechanism. Some relatively big grains can be observed however overall grain size was not changed remained between 8-10ASTM number. Twinning also can be observed for these specimens. On the other hand In Figure 6.14 in the dwell fatigue test surfaces, we can say crack propagation behavior has changed clearly since the topography of the fracture surfaces has distinctive features. And in “c” of Figure 6.14 shows that this change in the mechanism can be observable on the macro scale. This topographical change proves that crack propagation is changed from transgranular to mixed (trans+intergrarular) propagation.

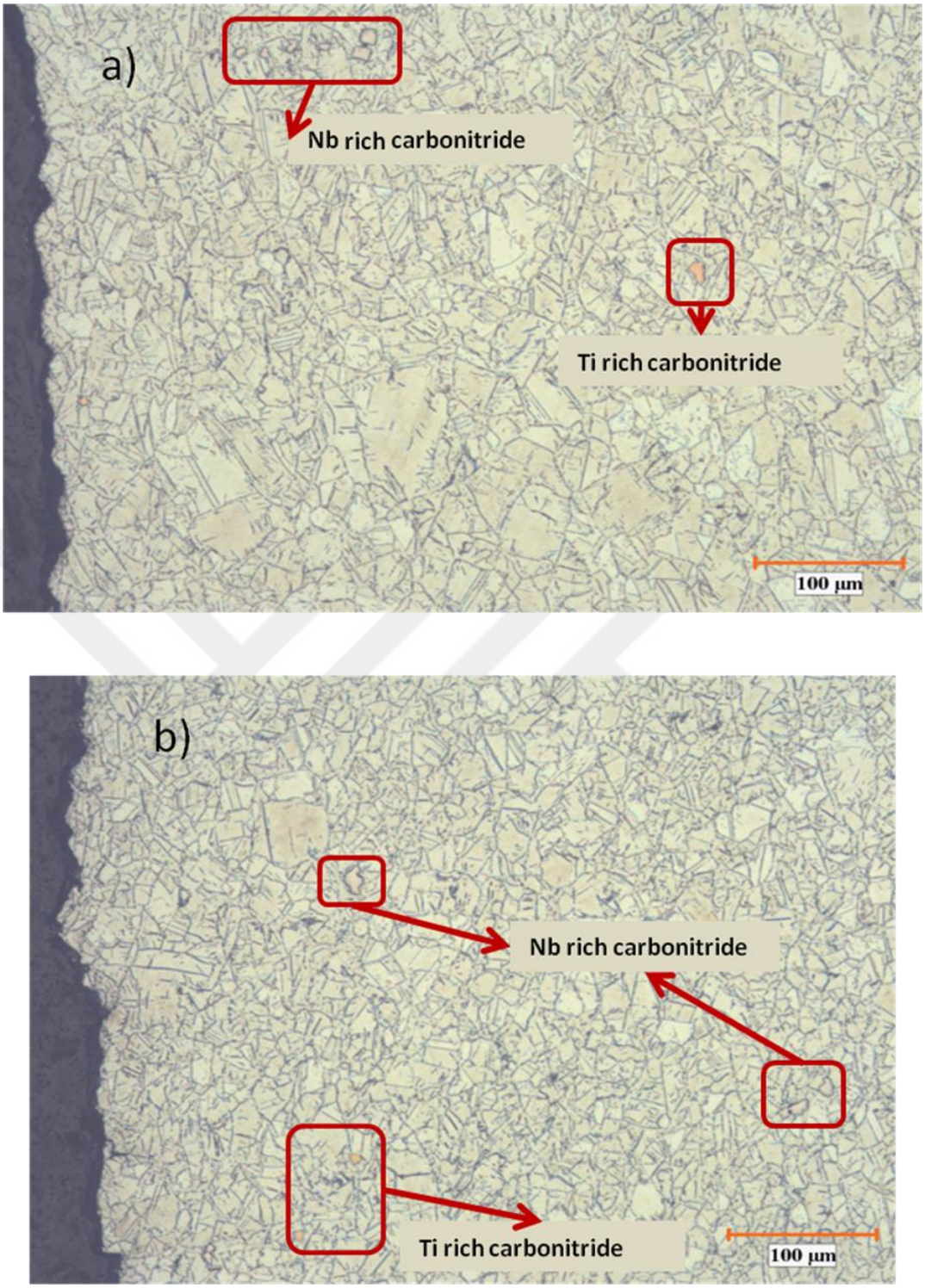


**Figure 6.13 :** Microstructural imaging of fracture surfaces a) 450 $^{o}$C Fatigue test 598Mpa 1.08 normalized cycles to failure b) 450 $^{o}$C Fatigue test 598Mpa 1.18 normalized cycles to failure.

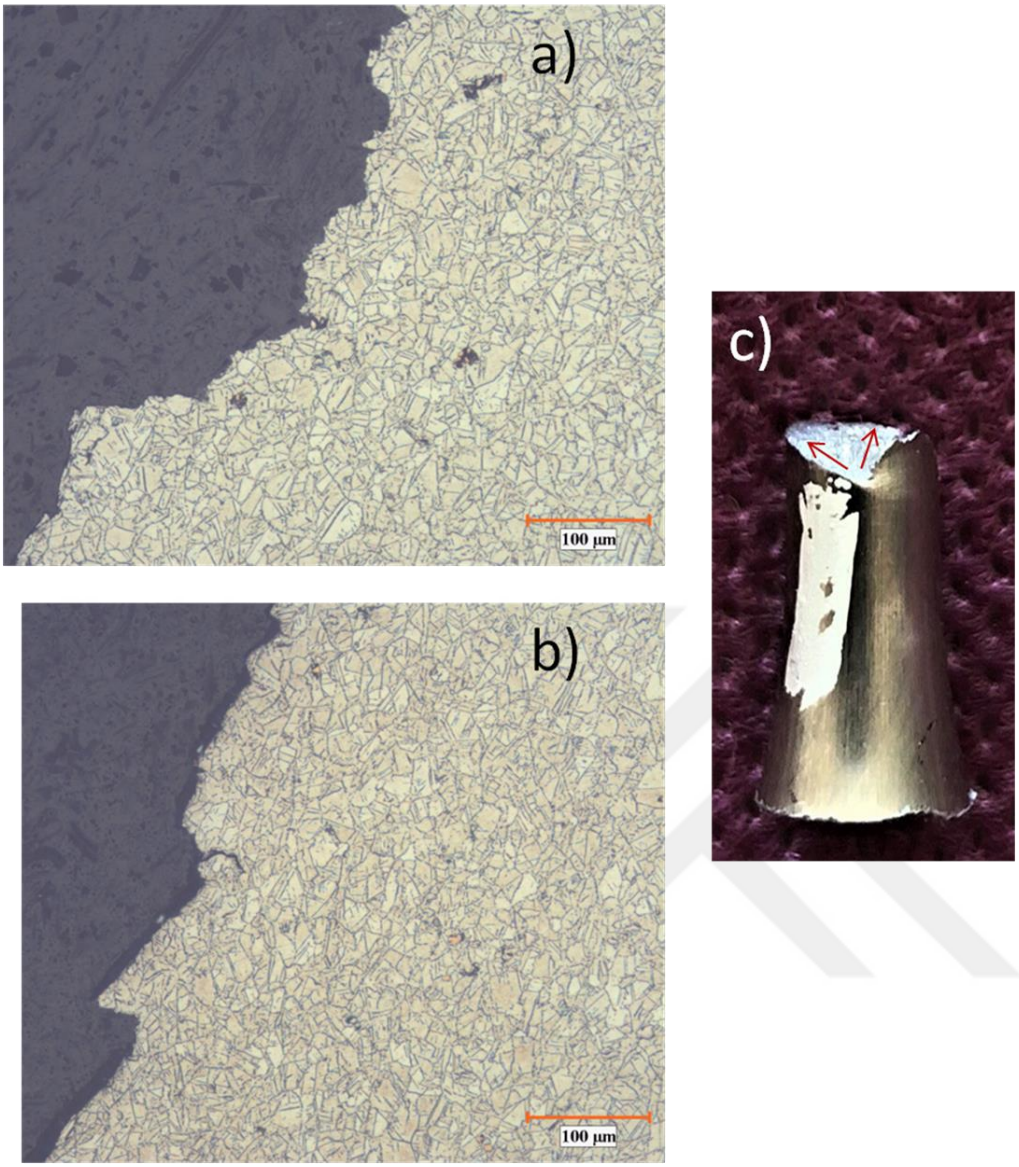


**Figure 6.14 :** Microstructural imaging of fracture surfaces a) 450 $^{o}$C Dwell Fatigue test 598Mpa 1.14 normalized cycles to failure b) 450 $^{o}$C Dwell Fatigue test 598Mpa 1.11 normalized cycles to failure c) Macro monitoring of a.

For further investigation of crack initiation and propagation, SEM monitoring is applied. In these observations, the aim was to detect some different features. Since the microstructural examinations lead to change in transgranular to intergranular propagation. In SEM analysis more quasi cleavage and facet type fracture features are expected. In Figure 6.15 dwell fatigue test and non-dwell fatigue test is compared in crack propagation zones. Both specimen surfaces are showing fatigue striations intensively means that the dominant fracture element is fatigue. Also, crack branching can be observed in both conditions. For these test conditions, it can be said that dwell application has no significant effect. As mentioned in NCR values in Figure 6.9 771Mpa is no dwell sensitive condition this observation supports this result.

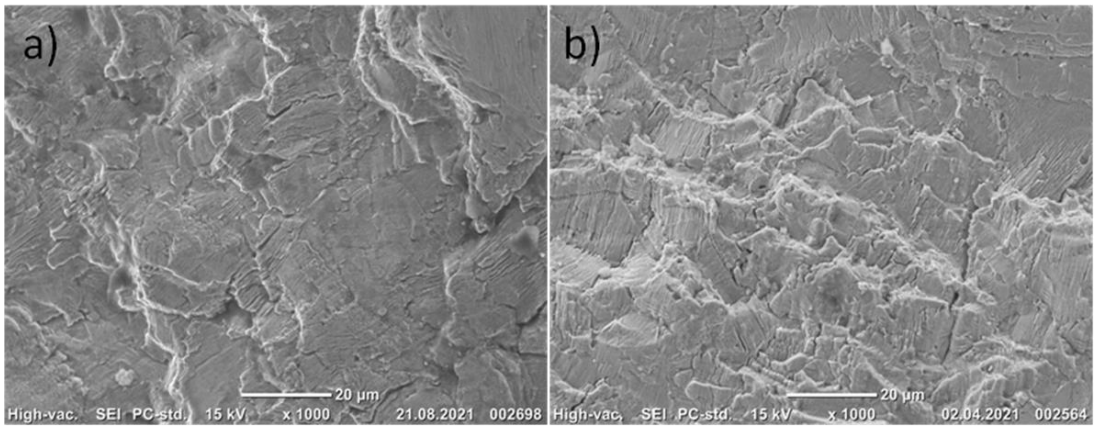


**Figure 6.15 :** SEM imaging of fracture surfaces a) 450 ºC Fatigue test 771Mpa 0.91 normalized cycles to failure b) 450 ºC Dwell Fatigue test 771Mpa 0.96 normalized cycles to failure.

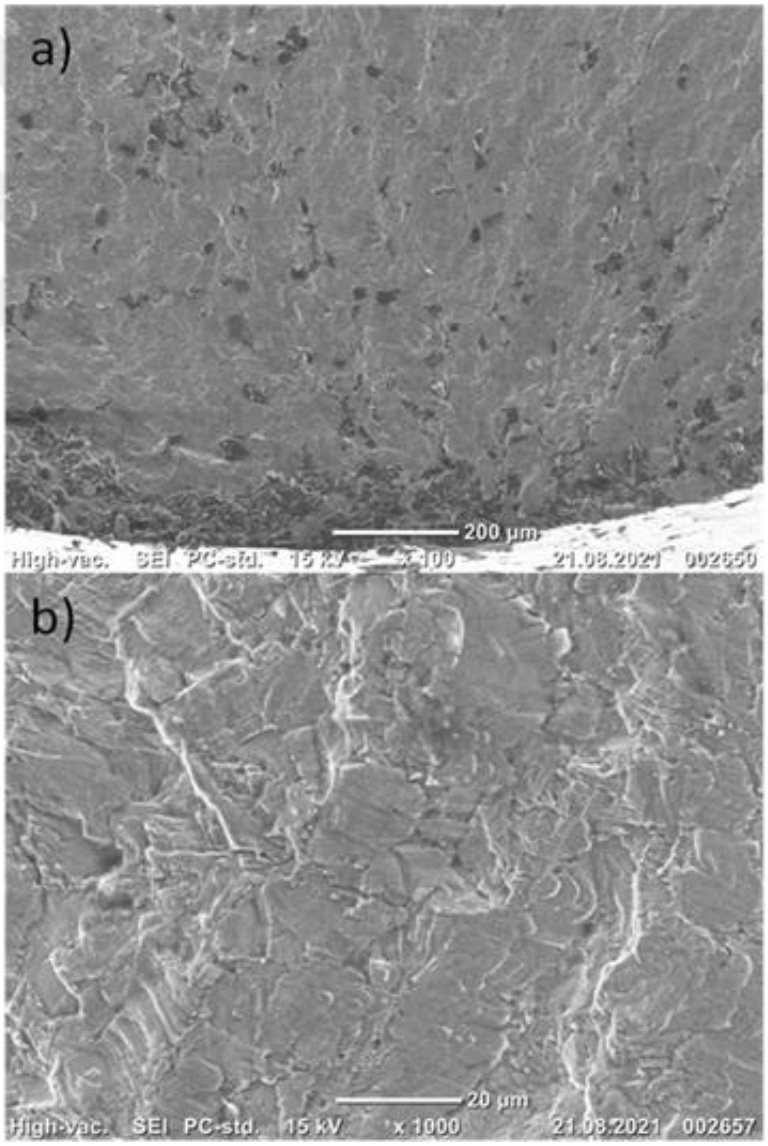


**Figure 6.16 :** SEM imaging of fracture surfaces of fatigue test at room temperature 560Mpa 1.26 normalized cycles to failure a) crack initiation zone b) crack propagation zone.

As mentioned in previous paragraphs, higher NCR conditions are observed in lower stress applications. At elevated temperatures, life results increase and failure has not been observed. But at room temperature life results are decreased drastically. In Figure 6.16, a non-dwell room temperature fatigue fracture surface is given. In this figure single crack initiation zone at the surface is observed and in the crack propagation region fatigue striations can be observed. In Figure 6.17, the topography and feature of the crack initiation site are different from Figure 6.16 in the dwell fatigue test more smooth crack paths and more quasi cleavage type features are observed. In the crack propagation site fatigue striations can be observed however quasi cleavage features are more distinct.

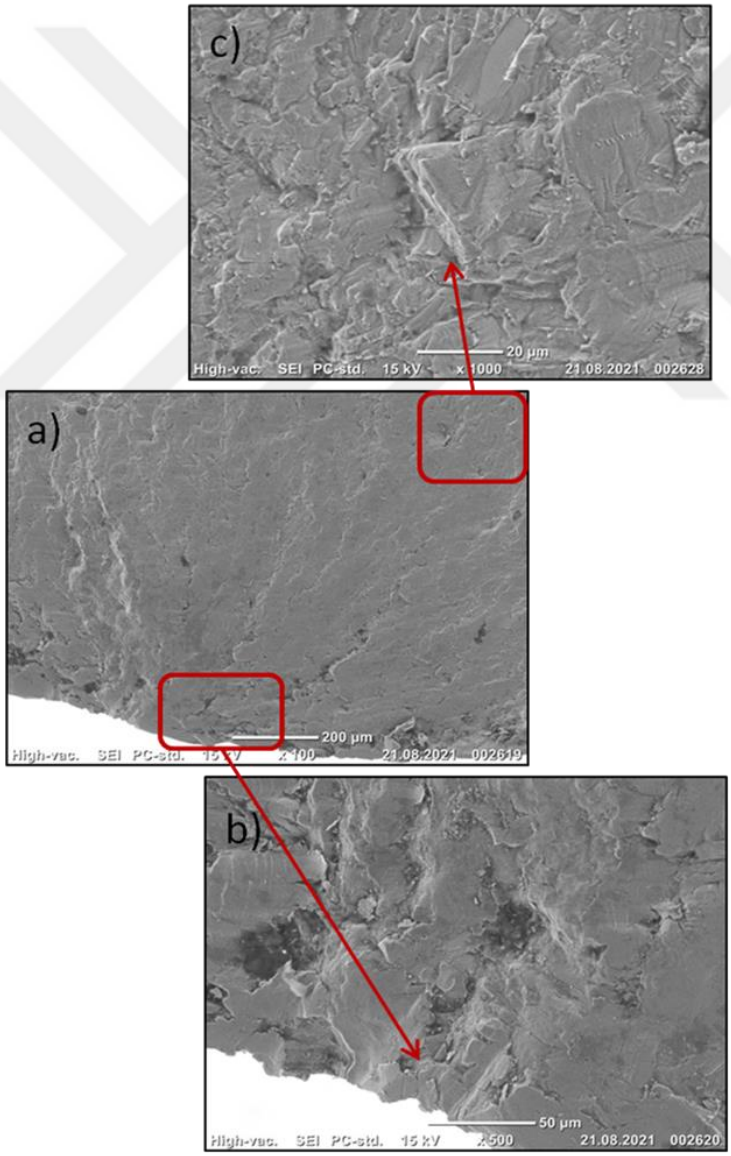


**Figure 6.17 :** SEM imaging of fracture surfaces of dwell fatigue test at room temperature 560Mpa 1.21 normalized cycles to failure a) crack initiation and propagation zone b) crack initiation zone c) crack propagation zone.

Another room temperature dwell fatigue failure surface is given in Figure 6.18**.** Unlike the other fracture surfaces in this specimen failure, it seems to have occurred more catastrophically. And from “a” and “b” shearing can be seen. At the crack propagation phase, quasi cleavage features are more visible additional to that, fatigue striations can be observed too. That means failure is not fully fatigue-dependent plasticity also can be considered.

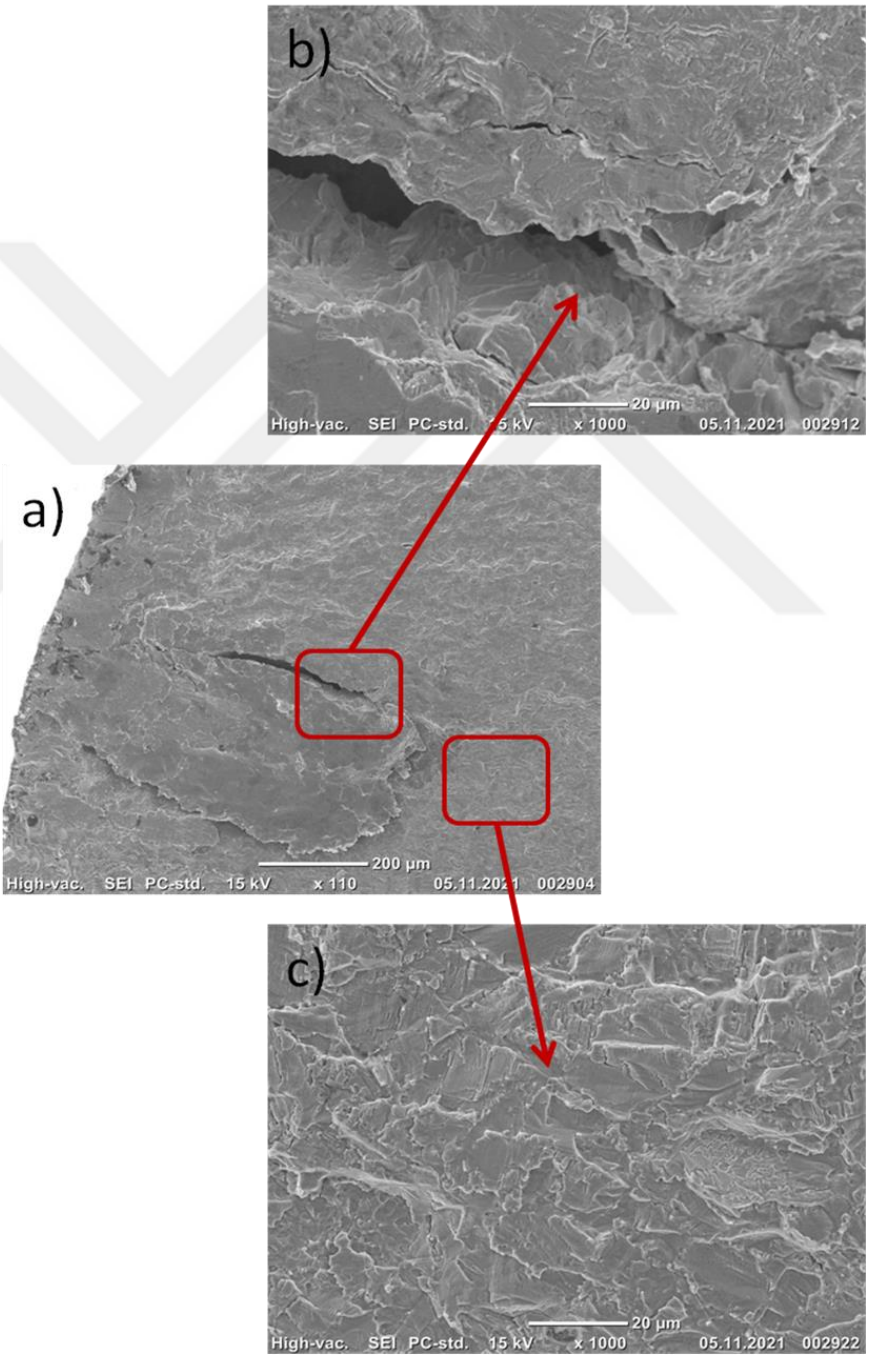


**Figure 6.18 :** SEM imaging of fracture surfaces of dwell fatigue test at room temperature 560Mpa 1.15 normalized cycles to failure a) crack initiation zone b) main crack zone c) crack propagation zone.

It is observed that dwell periods that caused an increase in life at 450ºC in terms of best fit curves, interestingly decreased life results nearly 60 percent at room temperature condition. And with examining the fracture surface with SEM imaging it is clearly seen that dwell application caused more catastrophic failure. Unlike 450 ºC temperature tests, at room temperature dwell application, quasi cleavage features are more visible. This might be because of active slip bands and dislocation mobility. Since the temperature is low and dislocation movement is restricted at a limited amount of slip bands, internal stresses can be accumulated more easily causing early failures. At elevated temperature with current observations, there is no grain size change and there is no change of materials plastic capability after fatigue and dwell fatigue tests. This means that it can not be related to an increase in life to the recovery mechanism. In addition to that Inconel 718 is a low stacking fault energy material means that the material requires higher temperatures or higher deformations to observe recovery [56]. High-stress application zones are not dwell-sensitive conditions. Softening is observed at near fracture locations.

The increase in life can be explained by different mechanisms. In literacy works different mechanisms are observed to arrest crack growth and cause crack closure such as; plasticity induce crack blunting, oxide induce crack arrest, mechanical closure. From our observations with softening increase in plasticity at the crack tips are highly possible to lead crack progpagation arrest. Crack closure and local plastically deformed zone which is a high energy zone and hardens the crack to propagate, at lower stress levels this mechanism is most likely to increase the material's pure bending fatigue life.

## 7. CONCLUSION

In this work load controlled rotating bending fatigue tests are performed under 2 different temperatures and dwell conditions. Additional to that hardness of Vickers measurements, nanoindentation, SEM monitoring, and optical microscopy visualizations are performed. As a result of these works following conclusions can be reached;

- Inconel718 pure bending fatigue life is highly affected by temperature, increasing in temperature decreases the fatigue life.
- Inconel718 material shows softening under cyclic loadings through the fracture surface. Softening can be affected by temperature.
- Dwell application has no decreasing effect to Inconel718 fatigue behaviour under bending at 450 $^{o}$C.
- At 450 $^{o}$C dwell application on Inconel718 material is stress-dependent, dwell sensitivity is observed at lower stress levels.
- At room temperature, dwell application at lower stresses showed a reduction in life.
- With dwell application fracture characteristics are observed to change from transgranular to mixed feature.
- Dwell sensitive stress regions are not favorable for recovery and recrystallization since there is no grain refinement and an increase in toughness is observed.

In the light of these works, it can be said that unexpectedly the detrimental effects of an increase in temperature and dwell loading have not been observed. Plasticity-induced crack closure is most likely to explain this increase in life.

## REFERENCES


[1] **M. J. Donachie and S. J. Donachie,** "SUPERALLOYS A Technical Guide Second Edition Superalloys: A Technical Guide (#06128G) www.asminternational.org," 2002. doi: 10.1361/stgs2002p011.

[2] **G. W. Meetham,** "Trace elements in superalloys–an overview," *Metals Technology*, vol. 11, no. 1, pp. 414–418, Jan. 1984, doi: 10.1179/030716984803275188.

[3] **"Aerospace materials: past, present and future,"** in *Introduction to Aerospace Materials*, Elsevier, 2012, pp. 15–38. doi: 10.1533/9780857095152.15.

[4] **W. Betteridge and S. W. K. Shaw,** "Development of superalloys," vol. 3, p. 13, 1987.

[5] **R. E. Smallman and R. J. Bishop,** *Modern physical metallurgy and materials engineering: science, process, applications*, 6th ed. Oxford ; Boston: Butterworth Heinemann, 1999.

[6] **A. J. Goodfellow,** "Strengthening mechanisms in polycrystalline nickel-based superalloys," *Materials Science and Technology*, vol. 34, no. 15, pp. 1793–1808, Oct. 2018, doi: 10.1080/02670836.2018.1461594.

[7] **D. K. Ganji and G. Rajyalakshmi,** "Influence of Alloying Compositions on the Properties of Nickel-Based Superalloys: A Review," in *Recent Advances in Mechanical Engineering*, H. Kumar and P. K. Jain, Eds. Singapore: Springer Singapore, 2020, pp. 537–555. doi: 10.1007/978-981-15-1071-7_44.

[8] **M. Jambor, O. Bokůvka, F. Nový, L. Trško, and J. Belan,** "Phase Transformations in Nickel base Superalloy Inconel 718 during Cyclic Loading at High Temperature," *Production Engineering Archives*, vol. 15, no. 15, pp. 15–18, Jun. 2017, doi: 10.30657/pea.2017.15.04.

[9] **S. Patel, J. deBarbadillo, and S. Coryell,** "Superalloy 718: Evolution of the Alloy from High to Low Temperature Application," in *Proceedings of the 9th International Symposium on Superalloy 718 & Derivatives: Energy, Aerospace, and Industrial Applications*, E. Ott, X. Liu, J. Andersson, Z. Bi, K. Bockenstedt, I. Dempster, J. Groh, K. Heck, P. Jablonski, M. Kaplan, D. Nagahama, and C. Sudbrack, Eds. Cham: Springer International Publishing, 2018, pp. 23–49. doi: 10.1007/978-3-319-89480-5_2.

[10] **Inconel alloy 718 special metals corporation.** (n.d.). https://www.specialmetals.com/documents/technicalbulletins/inconel/inconelalloy718.pdf

[11] **T. Nicholas,** *High cycle fatigue: a mechanics of materials perspective*. Oxford: Elsevier, 2006.

[12] **A. A. Azeez,** "MECHANICAL ENGINEERING AND PRODUCTION TECHNOLOGY," p. 32.

[13] **A. Nieslony, C. Dsoki, H. Kaufmann, and P. Krug,** "New method for evaluation of the Manson–Coffin–Basquin and Ramberg–Osgood equations with respect to compatibility," *International Journal of Fatigue*, vol. 30, no. 10–11, pp. 1967–1977, Oct. 2008, doi: 10.1016/j.ijfatigue.2008.01.012.

[14] **T. V. Duggan and J. Byrne,** *Fatigue as a Design Criterion*. London: Macmillan Education UK, 1977. doi: 10.1007/978-1-349-03222-8.

[15] **X. Yan, X. Chen, R. Sun, Y. Deng, L. Lin, and J. Nie,** "Investigation on Material's Fatigue Property Variation Among Different Regions of Directional Solidification Turbine Blades—Part I: Fatigue Tests on Full Scale Blades," *Journal of Engineering for Gas Turbines and Power*, vol. 136, no. 10, p. 102502, Oct. 2014, doi: 10.1115/1.4027928.

[16] **P. P. Milella,** *Fatigue and Corrosion in Metals*. Milano: Springer Milan, 2013. doi: 10.1007/978-88-470-2336-9.

[17] **"High cycle fatigue (HCF) testing of steel for Federal Aviation Administration (FAA) part qualification,"** p. 114.

[18] **U. Muralidharan and S. S. Manson,** "A Modified Universal Slopes Equation for Estimation of Fatigue Characteristics of Metals," *Journal of Engineering Materials and Technology*, vol. 110, no. 1, pp. 55–58, Jan. 1988, doi: 10.1115/1.3226010.

[19] **E08 Committee,** "Practice for Statistical Analysis of Linear or Linearized Stress-Life (S-N) and Strain-Life (-N) Fatigue Data," ASTM International. doi: 10.1520/E0739-10R15.

[20] **Snedecor, W. G.; Cochran, W. G.** Statistical Methods, 8th ed.; Iowa State University Press / Ames, 536.

[21] **R. L. Mason, R. F. Gunst, and J. L. Hess,** *Statistical design and analysis of experiments: with applications to engineering and science*, 2nd ed. New York: J. Wiley, 2003.

[22] **J. Spindel and E. Haibach,** "The method of maximum likelihood applied to the statistical analysis of fatigue data," *International Journal of Fatigue*, vol. 1, no. 2, pp. 81–88, Apr. 1979, doi: 10.1016/0142-1123(79)90012-4.

[23] **J. Schijve,** "A NORMAL DISTRIBUTION OR A WEIBULL DISTRIBUTION FOR FATIGUE LIVES," *Fat Frac Eng Mat Struct*, vol. 16, no. 8, pp. 851–859, Aug. 1993, doi: 10.1111/j.1460-2695.1993.tb00124.x.

[24] **J. F. Barbosa, J. A. Correia, R. Freire Júnior, S.-P. Zhu, and A. M. De Jesus,** "Probabilistic S-N fields based on statistical distributions applied to metallic and composite materials: State of the art," *Advances in Mechanical Engineering*, vol. 11, no. 8, p. 168781401987039, Aug. 2019, doi: 10.1177/1687814019870395.

[25] **P. Strzelecki and T. Tomaszewski,** "Application of Weibull distribution to describe S-N curve with using small number specimens," Fojutowo, Poland, 2016, p. 020007. doi: 10.1063/1.4965939.

[26] ***A Unified Statistical Methodology for Modeling Fatigue Damage*.** Dordrecht: Springer Netherlands, 2009. doi: 10.1007/978-1-4020-9182-7.

[27] **I. Kayes, J. Deb, P. Comeau, and S. Das,** "Comparing normal, lognormal and Weibull distributions for fitting diameter data from Akashmoni plantations in the north-eastern region of Bangladesh," *Southern Forests: a Journal of Forest Science*, vol. 74, no. 3, pp. 175–181, Sep. 2012, doi: 10.2989/20702620.2012.717409.

[28] **D. Kundu and A. Manglick,** "Discriminating between the Weibull and log-normal distributions," *Naval Research Logistics*, vol. 51, no. 6, pp. 893–905, Sep. 2004, doi: 10.1002/nav.20029.

[29] **J. Durbin and G. S. Watson,** "Testing for serial correlation in least squares regression. HI," p. 19.

[30] **Department of Management and Engineering,** Solid Mechanics, Linköping University, Sweden and E. Storgärds, *High Temperature Fatigue Crack Growth in a Ni-based Superalloy : Modelling Including the Interaction of Dwell Times*. Linköping University Electronic Press, 2015. doi: 10.3384/diss.diva-121012.

[31] **S. S. Manson and U. Muralidharan,** "FATIGUE LIFE PREDICTION IN BENDING FROM AXIAL FATIGUE INFORMATION," *Fat Frac Eng Mat Struct*, vol. 9, no. 5, pp. 357–372, May 1987, doi: 10.1111/j.1460-2695.1987.tb00462.x.

[32] **J. Belan, L. Kuchariková, E. Tillová, D. Závodská, and M. Chalupová,** "Effect of Fatigue Loading Mode on 718 Alloy Fatigue Properties," *Period. Polytech. Transp. Eng.*, vol. 47, no. 4, pp. 335–341, May 2018, doi: 10.3311/PPtr.12114.

[33] **M. Abikchi, J. Crepin, A. Longuet, C. Mary, and A. Pineau,** "Fatigue life and initiation mechanisms in wrought Inconel 718 DA for different microstructures," p. 12, 2013.

[34] **Kawagoishi, Chen, and Nisitani,** "Fatigue strength of Inconel 718 at elevated temperatures," *Fat Frac Eng Mat Struct*, vol. 23, no. 3, pp. 209–216, Mar. 2000, doi: 10.1046/j.1460-2695.2000.00263.x.

[35] **A. Pineau and S. D. Antolovich,** "High temperature fatigue of nickel-base superalloys – A review with special emphasis on deformation modes and oxidation," *Engineering Failure Analysis*, vol. 16, no. 8, pp. 2668–2697, Dec. 2009, doi: 10.1016/j.engfailanal.2009.01.010.

[36] **J. Wang *et al.*,** "Microstructure Heredity of Inconel 718 Nickel-Based Superalloy during Preheating and Following Deformation," *Crystals*, vol. 10, no. 4, p. 303, Apr. 2020, doi: 10.3390/cryst10040303.

[37] **G. E. Korth,** "Effects of Various Parameters on the Fatigue Life of Alloy 718," in *Superalloys 718, 625 and Various Derivatives (1991)*, 1991, pp. 457–476. doi: 10.7449/1991/Superalloys_1991_457_476.

[38] **K. J. Miller and D. J. Hatter,** "Increases in fatigue life caused by the introduction of rest periods," *Journal of Strain Analysis*, vol. 7, no. 1, pp. 69–73, Jan. 1972, doi: 10.1243/03093247V071069.

[39] **S.-H. Kim,** "THE EFFECT OF INTERMITTENT REST PERIODS AT ELEVATED TEMPERATURES ON THE FATIGUE PROPERTIES OF 4140 STEEL," in *Mechanical Behaviour of Materials*, Elsevier, 1984, pp. 825–831. doi: 10.1016/B978-1-4832-8372-2.50105-6.

[40] **W.-Y. Chu, C.-M. Hsiao, and T.-H. Liu,** "FATIGUE UNDER CYCLIC COMPRESSIVE LOAD," *Fat Frac Eng Mat Struct*, vol. 7, no. 4, pp. 279–284, Oct. 1984, doi: 10.1111/j.1460-2695.1984.tb00196.x.

[41] **U. Krupp,** "Dynamic Embrittlement — Time–dependent Quasi–brittle Intergranular Fracture at High Temperatures," *International Materials Reviews*, vol. 50, no. 2, pp. 83–97, Mar. 2005, doi: 10.1179/174328005X14320.

[42] **X. B. Liu,** "FATIGUE CRACK PROPAGATION OF Ni-BASE SUPERAIJ..OYS," p. 10.

[43] **D. Gustafsson,** Link??pings universitet, and Institutionen f??r ekonomisk och industriell utveckling, "High temperature fatigue crack propagation behaviour of Inconel 718," Department of Management and Engineering, Link??ping University, Link??ping, 2012.

[44] **E. Storgärds, J. Saarimäki, K. Simonsson, S. Sjöström, T. Månsson, and J. Moverare,** "Influence of superimposed vibrational load on dwell time crack growth in a Ni-based superalloy," *International Journal of Fatigue*, vol. 87, pp. 301–310, Jun. 2016, doi: 10.1016/j.ijfatigue.2016.02.018.

[45] **B. Pieraggi and J. F. Uginet,** "Fatigue and Creep Properties in Relation with Alloy 718 Microstructure," in *Superalloys 718, 625, 706 and Various Derivatives (1994)*, 1994, pp. 535–544. doi: 10.7449/1994/Superalloys_1994_535_544.

[46] **T. Goswami,** "Dwell Fatigue I : Damage Mechanisms," *High Temperature Materials and Processes*, vol. 19, no. 5, pp. 313–332, Aug. 2000, doi: 10.1515/HTMP.2000.19.5.313.

[47] **D. Gustafsson, J. J. Moverare, K. Simonsson, and S. Sjöström,** "Modeling of the Constitutive Behavior of Inconel 718 at Intermediate Temperatures," *Journal of Engineering for Gas Turbines and Power*, vol. 133, no. 9, p. 094501, Sep. 2011, doi: 10.1115/1.4002913.

[48] **J. Saarimäki, J. Moverare, R. Eriksson, and S. Johansson,** "Influence of overloads on dwell time fatigue crack growth in Inconel 718," *Materials Science and Engineering: A*, vol. 612, pp. 398–405, Aug. 2014, doi: 10.1016/j.msea.2014.06.068.

[49] **T. Goswami and H. Hanninen,** "Dwell effects on high temperature fatigue behavior Part I," p. 17, 2001.

[50] **L. Zhong, H. Hu, Y. Liang, and C. Huang,** "High Cycle Fatigue Performance of Inconel 718 Alloys with Different Strengths at Room Temperature," *Metals*, vol. 9, no. 1, p. 13, Dec. 2018, doi: 10.3390/met9010013.

[51] **D. Texier *et al.*,** "Crack initiation sensitivity of wrought direct aged alloy 718 in the very high cycle fatigue regime: the role of non-metallic inclusions," *Materials Science and Engineering: A*, vol. 678, pp. 122–136, Dec. 2016, doi: 10.1016/j.msea.2016.09.098.

[52] **H. Wang, R. Li, M. Zhou, J. Cedelle, Z. Huang, and Q. Wang,** "Grain boundary sliding mechanism in plastic deformation of nano-grained YAG transparent ceramics: Generalized self-consistent model and nanoindentation experimental validation," *Journal of the European Ceramic Society*, vol. 37, no. 7, pp. 2705–2715, Jul. 2017, doi: 10.1016/j.jeurceramsoc.2017.02.010.

## APPENDICES

**APPENDIX A:** High Temperature Statistical Graphics and Tabulated Calculations

**APPENDIX A:** High Temperature Curve Fitting and Statistical calculations.


**Figure A.1 :** Box Plots of different model equations on High temperature fatigue test results.

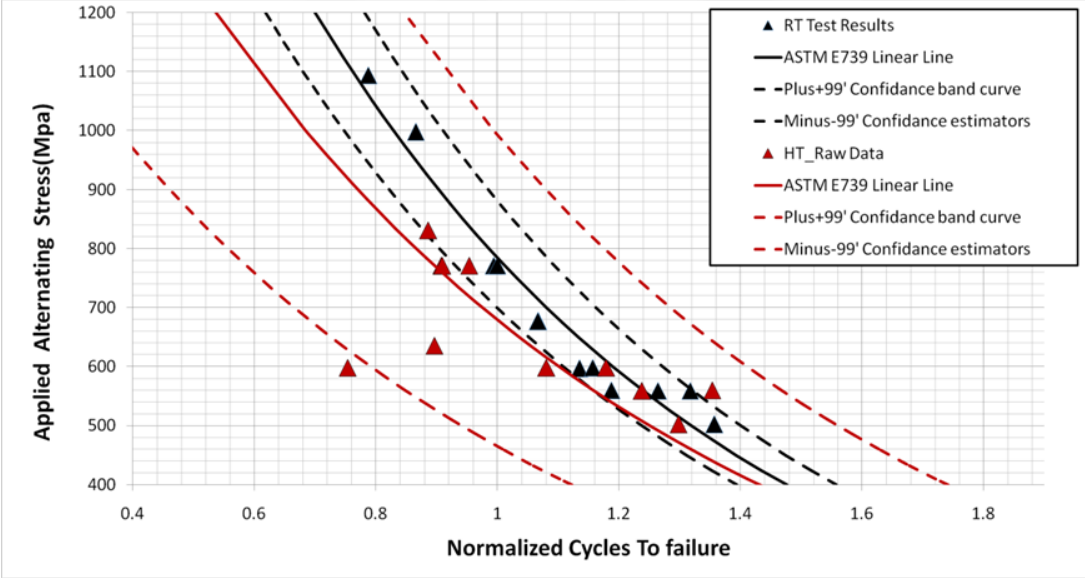


**Figure A.2 :** High Temperature and Room Temperature Best Fits and %99 confidance bands with test results.

**Table A.1 :** Calculated SSR & $R^2$ values for High temperature best fits.

| High Temperature Data Process Results | | |
|---|---|---|
| | Manson's Equal Slopes | ASTM_E739 |
| SSR | 4.032 | 4.032 |
| $R^2$ | 0.642 | 0.642 |

**Table A.2 :** Studendized T Outlier comparison according to Chapter 3 with significance of 0.05 for high temperature best fit.

| Critical TC | Absolute Ti | Applied Stress (Mpa) | Normalized Cycles to failure |
|---|---|---|---|
| 0.9786 | 1.100 | 635.7 | 0.8967 |
| | 2.443 | 598.2 | 0.7537 |
| | 0.073 | 771 | 0.9076 |
| | 0.162 | 598.2 | 1.0807 |
| | 0.395 | 771 | 0.9536 |
| | 0.552 | 559.2 | 1.238 |
| | 0.356 | 502 | 1.2979 |
| | 0.088 | 771 | 0.9096 |
| | 0.524 | 598.2 | 1.179 |
| | 1.366 | 560 | 1.3534 |
| | 0.352 | 831 | 0.8864 |

**Table A.3 :** Fitting Estimators according to linear ASTME739 Model of different test results.

| Model Equation: $\log N_f = A + B(\log \sigma)$ | | |
|---|---|---|
| Test Type | A | B |
| Room Temperature Fatigue | 28.78 | -8.20059 |
| High Temperature Fatigue | 29.68 | -8.74046 |
| High Temperature Dwell Fatigue | 36.86 | -11.13349 |

**CURRICULUM VITAE**

**Ad-Soyad** **:** Numan Berat YONDU

**ÖĞRENİM DURUMU:**

- **Lisans** **:** 2017,Yıldız Teknik Üniversitesi, Kimya ve Metalurji Fakültesi, Metalürji ve Malzeme Mühendisliği
- **Yüksek lisans** **:** 2017- devam, İstanbul Teknik Üniversitesi-Malzeme Mühendisliği

- **MESLEKİ DENEYİM VE ÖDÜLLER:**
- ERDEMİR DEMİR ÇELİK - Stajyer Mühendis(Sıcak Haddehane Kalite Metalürji ve Tufal üzerine çalışma+Sunum) 08.2016 - 09.2016
- Assan Alüminyum- Stajyer Mühendis(Dökümhane) 06.2016 - 07.2016
- 2018 Aralık ayı itibari ile TUSAS Motor Sanayii'de Malzeme ve Proses Geliştirme Müdürlüğünde Malzeme ve Proses Geliştirme Mühendisi olarak çalışmaya devam etmekteyim.